Design and Development of Elastic Scattering Spectroscopy (ESS)-based Probe for Breast Cancer Diagnosis

A DISSERTATION SUBMITTED IN PARTIAL FULFILMENT
FOR THE DEGREE OF

Master of Technology

IN THE
FACULTY OF ENGINEERING

BY

KIRTEYMAN SINGH RAJPUT (21760)
GUMMADI KUMAR RAJU (21125)

GUIDED BY

PROF. HARDIK J. PANDYA

DEPARTMENT OF ELECTRONIC SYSTEMS ENGINEERING
INDIAN INSTITUTE OF SCIENCE, BANGALORE

JUNE 2024

Synopsis

The research project aims to breast cancer diagnosis through the design and development of an elastic scattering spectroscopy (ESS)-based probe. Elastic scattering spectroscopy is a non-invasive optical technique that provides valuable structural or morphological changes in tissue. The proposed probe improves the sensitivity, specificity, and accuracy of breast cancer diagnosis by leveraging the unique capabilities of ESS.

The project begins with a comprehensive review of breast cancer, existing diagnostic techniques, and their limitations in detecting early-stage breast cancer. The project then delves into the principles of elastic scattering spectroscopy and its potential as a diagnostic tool. Through systematic experimentation and optimization, a custom-designed probe is developed to maximize the sensitivity and specificity of ESS for breast tissue diagnosis.

The research involves the diagnosis of breast cancer, the characterization of the probe's performance using phantom models, and optical properties measurements from *ex-vivo* tissue samples. The collected data is analyzed using algorithms to extract relevant information about tissue and identify potential biomarkers associated with breast cancer. A dedicated printed circuit board (PCB) has been meticulously designed for efficient data acquisition. The integration of this PCB facilitates seamless communication between the ESS probe and a custom-built graphical user interface (GUI) using Python. The GUI serves as a user-friendly platform for real-time data acquisition, providing pathologists/clinicians with a streamlined interface to monitor and analyze the obtained sample points.

Acknowledgements

We extend our sincere gratitude to Prof. Hardik J. Pandya, our esteemed Guide, for his unwavering support and mentorship throughout our master's program. His expertise, guidance, and patience have been invaluable, playing a pivotal role in the success of this project. We are truly grateful for the opportunity to learn and grow under his supervision. We are also grateful to Dr.Gayatri Gogoi from Assam Medical College, Assam for providing us the *ex-vivo* breast tissues for the experiments.

Our heartfelt appreciation goes to Mohammed Arif Kamal for his insightful guidance, which proved instrumental in shaping our project and crafting this thesis. His wisdom and support have been crucial to our academic journey, and we are grateful for his impactful contributions.

We would also like to express our thanks to Ajay A Krishnan for his generous provision of resources and unwavering support. Their collaborative efforts have greatly enriched our research endeavor, contributing significantly to the successful completion of this project.

Collectively, the guidance and support from these individuals have been indispensable in our academic and research pursuits, and we sincerely appreciate their contributions to our scholarly endeavors.

Contents

List of Figures

List of Tables

Chapter 1

Pre-study

The handheld breast cancer diagnosis and margin assessment system market is still in the early stages of its life cycle. Several diagnosis and margin assessment tools are currently available, but there is still a significant need for innovation, accuracy, sensitivity, and usability improvement. The marketplace is global in scope. However, the availability and adoption of these tools may vary by region, depending on factors such as healthcare infrastructure, regulatory environment, and patient preferences.

1.1 Background

Cancer is a disease in which cancer (malignant) cells develop in a tissue. One in eight women is diagnosed with breast cancer in her lifetime. The cause of breast cancer is rarely unknown, but it is caused by damage to the cell's DNA [4]. Benign tumors are not generally aggressive towards surrounding tissue but may cause pain and other problems. While malignant tumors are cancerous tissues that grow aggressively, invade, and damage the surrounding tissue. Sometimes, cancer cells spread to adjacent parts or other parts of the body through the lymph system or the bloodstream and form a secondary tumor called metastatic cancer. These tumors are graded based on the likelihood of spread and their severity. Tumors range from one to three grades, viz low grade, intermediate grade, and high grade.

1.1.1 Breast anatomy

The breast (also known as the mammary gland) is a highly complex organ in the human body. The internal structure of female breast tissue is illustrated in figure 1.1. Men and women both have breasts, but women have more breast tissue than men [5]. The female breast comprises the following:

- Lobules that produce breast milk.
- Ducts that carry milk to the nipple.
- Fatty (adipose) and connective (fibrous) tissue surround the lobules and ducts.

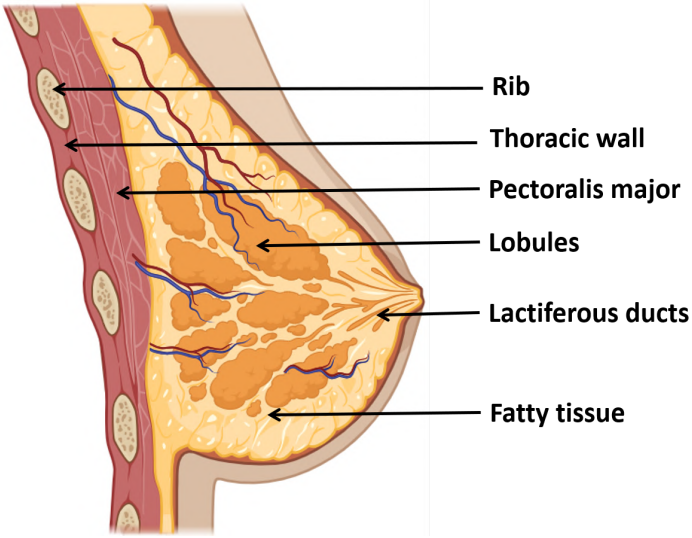

Figure 1.1: Internal structure of the breast.

(A) **Fatty (adipose) tissue and connective (fibrous) tissue:**
The female breast largely comprises fat cells, also known as adipose tissue. Fatty tissues span from the collarbone to the underarm and extend to the middle of the ribcage. The proportion of adipose (fatty) tissue in the female breast increases as women age, especially after menopause.

(B) **Glandular tissue (lobules):**
A healthy female breast comprises 12-20 lobes or sections surrounding the nipples. Each of these lobes is made up of many smaller lobules, which are milk-producing glands in nursing women.

(C) **Milk (mammary) ducts:**
Milk ducts are small tube-like structures, or ducts that carry milk from glandular tissue (lobules) to the nipple. Milk ducts are the breast structures generally where the cancer begins to form.

(D) **Lymph nodes:**
Lymph nodes are integral to the lymphatic system and play a crucial role in the immune system by protecting the body against diseases and infections. Typically, there are approximately 15 to 30 lymph nodes in the breast area. The lymph nodes nearest the breast are located in the armpit, known as axillary nodes. The axillary nodes are often the initial site where breast cancer spreads beyond the breast.

1.1.2 Types of breast cancer

The female breast undergoes many changes over a lifetime. Most of the changes are driven by hormones [6]. The changes can be linked to the menstrual cycle, pregnancy, or the natural aging process. Most of these changes are not indicative of cancer. However, it is important to consult your doctor for an appropriate diagnosis.

Breast cancer cells are often fuelled by normal healthy chemicals such as estrogen, progesterone, and the HER2/neu gene. These chemicals are known as prognostic factors for breast cancer cells. Like the blood circulatory system, the lymphatic system transports disease-fighting cells and fluids. The growth of cancer cells determines the type of breast cancer. Genetic or environmental factors, or a combination of both, could cause damage to the cell's DNA. Environmental and lifestyle risk factors can be avoided; typically, they are under the individual's control. Genetic risk factors that cannot be changed include the following:

- Sex, age, and race
- Personal health history, family history, and certain genome changes
- Menstrual and reproductive history, dense breast tissue

Breast cancer can be categorized based on the areas of the breast where it started [5], [6], [7] as illustrated in figure 1.2:

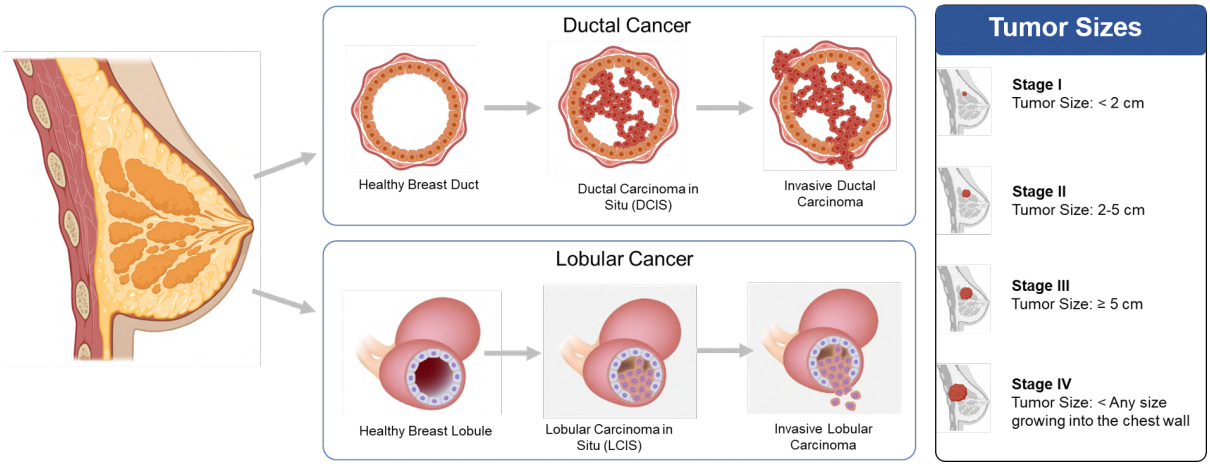

Figure 1.2: Types of breast cancer, ductal cancer, lobular cancer, and tumor sizes at different stages.

Noninvasive breast cancers:

- **Ductal carcinoma in situ (DCIS):** Ductal carcinoma in situ (DCIS) is a form of noninvasive breast cancer indicated by the presence of abnormal cells in the duct lining. These cells remain confined within the ducts and have not extended beyond the adjacent breast tissue. The initial phases of cancer development are termed ”carcinoma in situ,” with ”carcinoma” denoting cancer and ”in situ,” indicating that the tumor remains confined to its original location [8].

- **Lobular carcinoma in situ (LCIS):** Lobular carcinoma in situ (LCIS) is not classified as breast cancer but rather as a condition indicated by the presence of abnormal cells within the lobules of the breast. LCIS is typically highly manageable and rarely progresses to invasive cancer. However, having LCIS in one breast increases the likelihood of developing breast cancer in either breast [8].

Invasive breast cancers:

- **Invasive ductal carcinoma (IDC):** Invasive ductal carcinoma (IDC) is an invasive form of cancer wherein abnormal cancerous cells originating in the milk ducts infiltrate beyond these ducts and into surrounding breast tissue. IDC is the predominant form of breast cancer, constituting approximately 70-80% of all diagnosed cases of breast cancer [8].

- **Invasive lobular carcinoma (ILC):** Invasive lobular breast cancer (ILC) refers to invasive breast cancer originating in the lobules or the milk-producing glands of the breast

and extending into adjacent normal tissue. Representing the second most prevalent variety of breast cancer, invasive lobular breast cancer accounts for more than 10% of all invasive breast cancer cases. Unlike some other types of breast cancer, ILC might not exhibit distinct features on a mammogram, often necessitating the use of MRI for accurate detection [8].

Other types of breast cancer:

- **Inflammatory breast cancer (IBC):** Inflammatory breast cancer (IBC) manifests when cancerous cells invade the skin and lymphatic vessels of the breast. Characterized by its aggressive nature, IBC poses challenges in diagnosis compared to other breast cancer types and frequently affects younger women [8].
- **Metastatic Breast Cancer (MBC):** When breast cancer reappears in a different part of the body, whether months or years after the initial diagnosis and treatment (known as distant recurrence), it is termed metastatic breast cancer. Although a cure for metastatic breast cancer is not presently available, advancements in treatment have enabled many women to prolong their lives while managing the disease as a chronic condition, with an emphasis on enhancing quality of life as a primary objective [8].

1.1.3 Symptoms of breast cancer

Although a lump in the breast is a common symptom of breast cancer, not all breast cancers present with noticeable symptoms. Some lumps may be too small to be felt but can be detected through screening mammograms or other tests. Additionally, there are benign (noncancerous) conditions that can cause breast lumps, such as cysts (fluid-filled sacs) and fibroadenomas (lumps made of fibrous and glandular tissue).

Most breast changes are not due to cancer. However, it is crucial to see your doctor promptly if you notice any new lumps or unusual changes in your breasts. Early detection significantly increases the chances of successful treatment if breast cancer is diagnosed [9].

1.1.4 Diagnostic techniques

According to the American Cancer Society, the five-year survival rate of patients with breast cancer is 99%. Early detection of breast cancer includes self-examination, clinical breast examination, and mammography, as shown in figure 1.3

Breast self-examination is an early detection tool for checking for signs and symptoms of breast cancer. While a breast self-examination is useful, it should not replace usual mammography and clinical breast exams.

A healthcare professional performs a clinical breast examination, generally by your family physician or gynecologist. The most significant benefit of breast cancer screening is reduced mortality. A mammogram is an X-ray that examines breast tissue by ionizing radiation. Women aged 40 years and older should undergo mammogram exams every year. Diagnostic techniques such as X-ray mammography [5], sonography, and magnetic resonance imaging (MRI) [6] have reliability and capability issues in detecting tumors due to the heterogeneous media of breast tissue. X-ray mammography, the most common technique, measures the attenuation of X-rays with a sensitivity and specificity of 77% and 97%, respectively. An X-ray has a radiation risk. MRI reveals tissue properties by exciting and aligning the hydrogen atoms with the highest sensitivity between 93% and 100%. MRI is bulky, expensive, and time-consuming. Ultrasonography yields results with high sensitivity and specificity for detecting breast cancer. However, ultrasonography requires skilled labor and produces false positive results [7] compared to X-ray mammography.

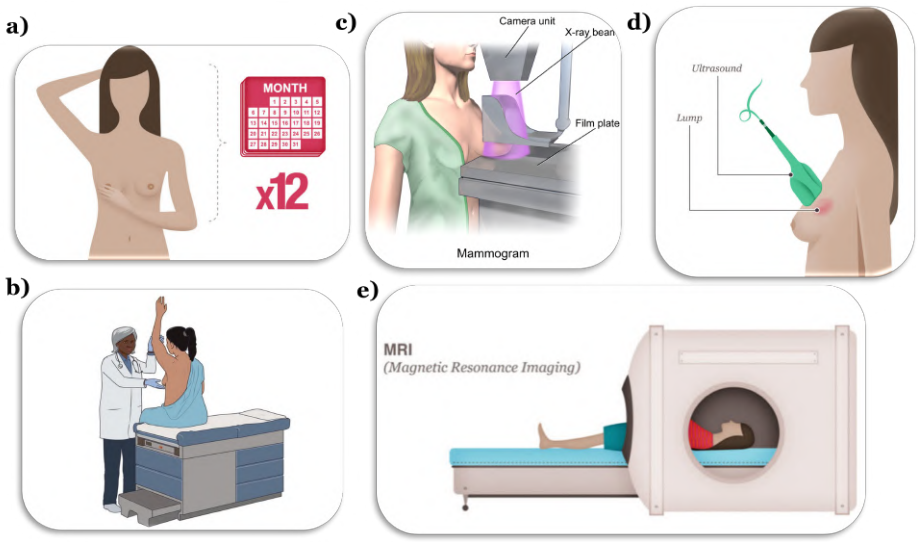

Figure 1.3: a) Breast Self-Exam, b) Clinical Breast Exam, c) Mammogram, d) Ultrasound, and e) MRI.

1.1.5 Elastic scattering spectroscopy (ESS) Probe

According to the Globocan 2022 report [10], breast cancer ranks second in incidence and fourth in mortality. This report indicates that the number of breast cancer cases is expected to increase significantly in the future. To support the diagnosis and treatment of this growing number of cases, technologies that can rapidly and accurately distinguish cancerous tissue from normal tissue are needed. A fast and reliable method for differentiating between adjacent normal and cancerous tissue will aid doctors and pathologists in diagnosing cancer. It will also benefit surgeons performing breast cancer surgeries, such as lumpectomies, by assisting them in margin assessment during the procedure. The aim of our system is to develop a platform that delineates cancerous tissue by using the principle of elastic scattering spectroscopy. The intraoperative probe is a medical device that utilizes the ESS technique to provide real-time assessment of breast cancer margins during surgery. The device is a portable handheld tool capable of scanning the tissue at the margins of the cancerous region. The probe is equipped with a multiwavelength LASER source (850nm, 980nm, 1270nm, and 1050nm) that interacts with the tissue via absorption and scattering phenomena, resulting in accurate margin detection. This allows for precise identification of cancerous tissue and helps to ensure that all diseased tissue is removed during surgery.

1.2 Functional aspects

The primary function of the proposed probe is to facilitate breast cancer diagnosis through the application of ESS technology. The system comprises a data acquisition unit, optic fibre bundles, and a personal computer that runs a customized user-friendly GUI for seamless interaction and real-time monitoring of the acquired data.

The integrated system aims to provide clinicians/pathologists with a comprehensive tool to analyze tissue, aiding early breast cancer diagnosis. The system also provides data processing and plot visualization capabilities through the GUI. The acquired measurements from the tissue sample are given to a data processing algorithm that extracts optical properties such as absorbance and scattering from the tissue sample. The GUI allows the user to keep track of all the measurements and delete the measurement if something goes wrong, providing complete control of the measurement procedure. It also helps to interpret and analyse the processed data, enhancing the diagnostic capabilities of the overall system.

Maintaining the relevant standards and protocols is paramount in developing this product.

Compliance with ethical guidelines for human subject research, data privacy regulations, and industry standards for medical devices ensures product reliability, safety, and ethical use in clinical settings. Additionally, data acquisition, processing, and interface design protocols contribute to the overall robustness and reliability of the proposed breast cancer diagnostic system.

1.3 Characteristics and performance

The system is designed to measure and monitor key optical parameters related to tissue microstructure. Primary parameters include reflectance, scattering coefficient, and absorbing coefficient of breast tissue. These parameters are critical for characterizing morphological structures and identifying potential abnormalities indicative of breast cancer. The system also controls the data acquisition process, ensuring the quality and integrity of the acquired optical characteristics.

The system is usually designed to meet high-performance standards for accurate and reliable breast cancer diagnosis. Performance requirements include real-time data acquisition capabilities, efficient data processing, and seamless GUI interaction. The system exhibits sensitivity and specificity in interpreting variations in scattering and absorption coefficients, ensuring precise identification of abnormal tissue.

Various factors can influence the product's performance, including ambient light conditions, variations in tissue optical properties, and potential noise sources during data acquisition. Careful consideration and mitigation strategies for these factors are essential to maintain the reliability and accuracy of the breast cancer diagnostic system.

1.4 User aspects

The technical competence of the user is a crucial consideration in the design and usability of the breast cancer diagnostic system. Given the specialized nature of elastic scattering spectroscopy (ESS) technology, users, typically healthcare professionals, should possess a certain level of technical proficiency. Training programs and user manuals are necessary to ensure that users are adequately equipped to operate the system, interpret results, and make informed clinical decisions. The system is designed for real-time monitoring and adjustment; constant interaction is necessary.

1.5 Environment aspects

The ambient temperature range of the system can be in the range from 20° to 45°, as LASER diodes have operation temperatures from -10° to 85°. The PCB, power adapter, and LASER diodes with SMA couplers are fixed rigid to the 3D case, such that in case of some pressure and vibration, the system remains stable.

1.6 Power supply

The product is designed to operate on a 220V, 50Hz supply voltage. The design ensures a continuous and reliable power supply without battery replacement or recharging. Operating from a power line simplifies the setup process for users and eliminates concerns about battery life or charging intervals. Additionally, it allows the product to draw consistent power levels, which is advantageous for applications requiring sustained operation over extended periods. The PCB components require $\pm$12V for the PDAPC4 detector, $\pm$9V for Op-amp in the photodetector circuit, and +5V for a cooling fan. To meet this power requirement, a power adapter EC4PS [11] from Thorlabs has been utilized, as shown in figure 1.4, and the input power for this adapter is a regular power line 220V. In the event of a power breakdown, the product will cease functioning until power is restored. Depending on the nature of the power failure and the system's design, there are protocols to handle unexpected power loss.

Figure 1.4: EC4PS power adapter.

The system employs surge protection mechanisms to safeguard against voltage spikes during power fluctuations. Furthermore, users are advised to have backup power, such as uninterrupt-

ible power supplies (UPS), to avoid the impact of power outages on critical operations. The product is engineered to operate within specific power consumption parameters to ensure compatibility with standard electrical infrastructure. Design optimizations focus on maximizing energy efficiency to minimize operating costs and environmental impact. Additionally, regulatory compliance with safety standards and power quality requirements may influence the design and performance of the product to ensure seamless integration with existing power distribution networks.

1.7 Safety

The equipment is intended for installation in locations where the supply voltages do not exceed 270V concerning the Earth. Such locations typically include standard residential, commercial, and industrial environments where the electrical infrastructure meets established voltage regulations and safety standards. Installations in these locations ensure compatibility with the prevailing electrical systems and mitigate the risk of voltage-related issues such as overloading, electrical shocks, or equipment damage. The maximum permissible exposure (MPE) time varies depending on the wavelength(850nm, 980nm, 1270nm, 1550nm). For exposure time of 100ns to 10s, MPE (Jm^{-2}) is 10403.157 for 850nm, 980nm, 1270nm, and 4211.875 for 1550nm provided t_{max} = 0.8s for P_{max} = 10mW.

1.8 Literature survey

ESS is also one of the techniques that have the potential for margin assessment during surgery. ESS uses light to probe the tissue and measure the scattering properties of the tissue at a microscopic level [12]. This technique has several advantages compared to other margin assessment techniques, which include:

- Real-time assessment: ESS provides real-time feedback during surgery, allowing the surgeon to assess the margin and adjust the surgical plan if necessary.
- Label-free: ESS is a noninvasive technique that does not require using contrast agents or tissue markers, making it safe and easy to integrate into existing surgical workflows.
- High sensitivity: ESS is highly sensitive to changes in tissue morphology, allowing it to detect even minor changes in tissue structure that may indicate cancerous cells.

- Low cost: ESS is relatively low-cost compared to other margin assessment techniques, making it accessible to a broader range of healthcare providers and patients.
- Minimal tissue damage: ESS does not cause any tissue damage, allowing the surgeon to preserve more healthy tissue and potentially reduce the need for re-excision surgeries.

Overall, ESS is a promising technique for cancer margin assessment that offers several advantages over other approaches. The marketplace for this tool is highly competitive, with several established companies and research organizations developing and testing various technologies. Some existing players in this space include MarginProbe, Lumicell, Verisante Aura, etc., as shown in figure 1.5. However, as the demand for more accurate and efficient margin assessment tools grows, there will likely be new entrants in the market. ESS has a high potential for cancer margin assessment during surgery. It's also advantageous compared to other methods because of real-time feedback, non-invasiveness, high sensitivity, low cost, and minimal tissue damage. However, further validation and testing are needed to demonstrate its clinical utility and effectiveness. Overall, the marketplace for breast cancer margin assessment tools is dynamic and evolving, focusing on developing technologies to improve patient outcomes and reduce the need for re-excision surgeries.

Several potential value additions can be made to fix the gaps in breast cancer margin assessment tools. This can involve technological improvements, product design, cost, and usability. These value additions help address existing market gaps, creating opportunities for innovation and growth.

- Development of new technologies: Research into emerging technologies, such as elastic scattering spectroscopy (ESS), can lead to the development of more accurate and sensitive margin assessment tools that can be used in real-time.
- Integration of machine learning: Incorporating AI and machine learning algorithms into margin assessment tools can help improve their accuracy and sensitivity over time, enabling more personalized treatment options for patients.
- User-centered design: User-centered design principles can be used to develop margin assessment tools that are easy to use and require minimal training, reducing the risk of errors or complications.
- Cost optimization: Focus on optimizing the cost of margin assessment tools to make them more accessible to a broader range of healthcare providers and patients.

Breast cancer margin assessment tools can offer significant value to targeted customers, including patients, healthcare providers, and insurers. These tools can help to improve the accuracy and efficiency of surgical procedures, reduce the need for re-excision surgeries, and ultimately improve patient outcomes. Furthermore, cost-effective and easy-to-use margin assessment tools can help to reduce the overall cost of care for breast cancer patients.

1.9 Product/market survey

- **Yearly growth rates, phase of the offering in its lifecycle (early/established/diminishing), geographical spread (increase/decline), etc.**
  Access to affordable healthcare for breast cancer diagnosis ensures that women receive timely and accurate diagnosis and treatment. According To GLOBOCAN reports [10], cancer cases will increase to 28.4 million in 2040. Globally, the number of breast cancer cases was 2,21,419 (11.7 % of all cancer cases). The breast cancer margin assessment tool marketplace will experience significant growth in the coming years. The increasing trend of incidence of breast cancer, rising awareness about early diagnosis, and the need for improved surgery will require these tools in the market. The market for these tools is still in the early stages of its lifecycle. While several margin assessment tools are currently available, there is still a significant need for innovation, accuracy, sensitivity, and usability improvement. The marketplace is global in scope. However, the availability and adoption of these tools may vary by region, depending on factors such as healthcare infrastructure, regulatory environment, and patient preferences.

- **Competition (existing or likely from players in the adjacent space).**
  There is significant competition in developing and marketing breast cancer margin assessment tools. Many companies and academic institutions are developing technologies, as shown in figure 1.5, and techniques to improve the sensitivity, specificity, and accuracy of margin assessment during lumpectomy surgeries. Some of the existing players in this space include:

  1. MarginProbe (Developed by Dune medical devices): MarginProbe is a handheld device that uses radio frequency technology to detect cancerous tissue in the surgical cavity during lumpectomy procedures. The device can provide real-time feedback to surgeons, enabling them to ensure that all cancerous tissue has been removed [13].

2. ClearEdge (Developed by ClearCut medical): ClearEdge is a noninvasive imaging system that uses radio frequency technology to detect the location of breast tumors and assess the margins in real time. The device can provide high-resolution images that enable surgeons to visualize the tumor and surrounding tissue during the lumpectomy procedure [14].
3. Endomag offers a system that uses magnetic nanoparticle technology (magseed marker) to guide surgeons during breast cancer surgery. The system includes a magnetic tracer and a handheld probe that can detect the tracer in real-time, allowing surgeons to identify the tumor margins precisely [15].
4. OncoRes Medical is developing a handheld device that combines ultrasound imaging and tissue analysis to provide real-time feedback to surgeons [16].
5. Verisante Aura - A technology developed by Verisante Technology that uses Raman spectroscopy to detect cancerous tissue during surgery [17].
6. Lumicell - A technology developed by Lumicell, Inc. that uses a fluorescent imaging agent to identify cancerous cells during surgery [18].

Figure 1.5: a) Clear Edge, b) Lumicell, c) Magseed, d) Margin Probe, and e) Verisanta Aura.

Table 1.1: Current implementations of similar medical devices in the market

S. No	Device	Company	Technology Used
1	Margin Probe	Dune Medical Devices	Radio Frequency
2	Clear Edge	Clear Cut Medicals	Radio Frequency
3	Magseed	Endomag	Magnetic Nanoparticle Technology
4	OncoRes	OncoRes Medical	Ultrasound Imaging
5	Verisante Aura	Verisante Technology	Raman Spectroscopy
6	Lumicell	Lumicell, Inc.	Fluorescent Imaging

1.10 User survey

The potential users of intraoperative probes based on elastic scattering spectroscopy (ESS) are surgical oncologists, pathologists, biomedical engineers, and researchers. The users are comprised of both technical and nontechnical professionals. Surgical oncologists and pathologists typically have a technical background, while biomedical engineers and researchers are also technically proficient. Users believe that the real-time ability of the ESS probe to assess breast cancer margins during surgery is valuable. They see it as a potential tool to improve surgical outcomes for patients by assisting in the identification of cancerous tissue. While users may desire additional features such as higher-resolution imaging or deeper tissue penetration, limitations in current technology may make these features difficult to implement. For example, achieving higher resolution may require significant advancements in sensor technology, which may not be feasible in the current design.

Users see ESS technology as a promising tool to improve surgical outcomes by aiding in identifying cancerous tissue during surgery. They express interest in utilizing ESS probes to assist in identifying cancerous tissue during surgery, highlighting the potential benefits it could offer in improving patient care. Users also recognize the importance of integrating the ESS probe technology as an option for surgeons, indicating a willingness to explore its implementation in their facilities. Users prioritize reliability, ease of use, and clinical efficacy when evaluating new medical technologies for implementation in their facilities. Users are interested in understanding how ESS probes measure up against other intraoperative imaging technologies, suggesting a desire to evaluate its performance relative to existing options.

Chapter 2

Study

Breast cancer is one of the leading causes of death in the female population worldwide. In terms of incidence, breast cancer ranks second, with 2,296,840 new cases worldwide in 2022 [10]. It is a highly prevalent cancer that predominantly affects the female population. According to the International Agency for Research on Cancer, in terms of mortality, breast cancer ranks fourth, causing 666,103 deaths worldwide in 2022.

The handheld breast cancer diagnosis and margin assessment system market is still in the early stages of its life cycle. Although several diagnostic and margin assessment tools are currently available, improvements in innovation, accuracy, sensitivity, and usability are still needed. The marketplace is global in scope. However, the availability and adoption of these tools may vary by region, depending on factors such as healthcare infrastructure, regulatory environment, and patient preferences. Elastic scattering spectroscopy (ESS) is also a technique that has the potential for the diagnosis of breast tissue during surgery. ESS uses light to probe breast tissue and measure the scattering properties of the tissue at the microscopic level. This technique has several advantages compared to other margin assessment techniques (i.e., X-ray mammography [19], MRI [20], and ultrasonography), which include real-time assessment, noninvasiveness, low cost, and minimal tissue damage.

The marketplace for this tool is highly competitive, with several established companies and research organizations developing and testing various technologies. Some existing companies in this space include MarginProbe, Lumicell, and Verisante Aura. However, as the demand for more accurate and efficient diagnostic and margin assessment tools is growing, there will likely be new entrants in the market.

ESS has high potential for cancer diagnosis and margin assessment during surgery. It is also

advantageous compared to other methods because of its real-time feedback, noninvasiveness, high sensitivity and specificity, low cost, and minimal tissue damage. However, further validation and testing are needed to demonstrate its clinical utility and effectiveness. Overall, the marketplace for breast cancer diagnosis and margin assessment tools is dynamic and evolving, with a focus on developing technologies to improve patient outcomes and reduce the need for re-excision surgeries.

2.1 Functional concept

The proposed intraoperative probe utilizes the ESS technique to provide real-time breast cancer diagnosis and margin assessment intraoperatively. The probe is a portable handheld tool capable of scanning tissue to confirm whether the tissue is malignant or benign. The probe has a multiwavelength LASER diode (850nm, 980nm, 1270nm, and 1550nm)[21, 22, 23, 24] that interacts with the breast tissue via absorption and scattering phenomena, resulting in accurate diagnosis and margin detection. This allows for precise identification of cancerous tissue and helps to ensure that all diseased tissue is removed during surgery. Surgical oncologists are potential users of this intraoperative probe based on ESS.

The probe consists of LASER light sources of wavelengths 850nm, 980nm, 1270nm, and 1550nm along with a photodetector PDAPC4 (Thorlabs) [25] with suitable bandwidth. A data acquisition module outside the probe tip managed the LASER diodes control sequence and the data acquisition from the photodetector. Arduino Mega is used as the microcontroller, and its analog and digital capabilities are utilized. The data acquisition module (microcontroller) is powered from the PC/laptop/Tablet using a connector, which simultaneously communicates with the Python-based GUI. The photodetector PDAPC4 is integrated with a monolithic, low-noise, precision trans-impedance amplifier for current-to-voltage conversion. Then, the obtained voltages are sent to the ADC peripheral of the microcontroller. The microcontroller converts the ADC voltage level to the corresponding voltage and communicates it with the user interface.

Key Features of the Intraoperative Probe:

1. Intraoperative probe based on the ESS technique.
2. The intraoperative probe is a handheld device that can scan the tissue to confirm the cancerous region.

3. Probe comprises multi-wavelength LASER light source (850nm, 980nm, 1270nm, and 1550nm) that illuminates and interacts with the tissue through absorption and scattering phenomena.

4. Reflected light from tissue gets detected by the photodiode PDAPC4.

5. The Data acquisition module is connected to a laptop using the UART interface to display a real-time assessment of the tissue.

6. Python-based GUI using Flask and Tkinter libraries in Python.

The functionality is depicted in a functional block digaram, as shown in figure 2.1.

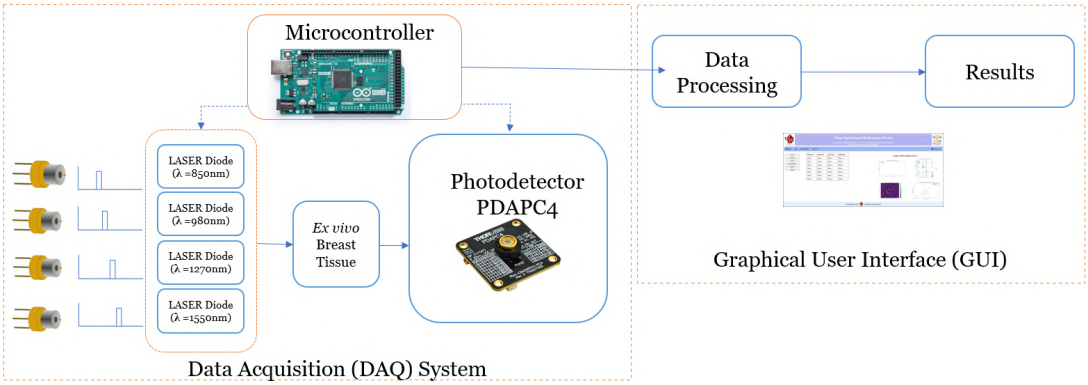

Figure 2.1: Functional block diagram.

2.2 Modules for ESS based probe

The entire system can be divided into three parts: 1) Source end that contains illumination sources and their driver and control ciruit. 2) Channel which consists of optic fibre bundles 3) Detector end comprises of a photodetector to measure the reflected light from the tissue sample.

2.2.1 Illumination sources

2.2.1.1 L850P010

The L850P010 from Thorlabs Inc. is a LASER diode with a wavelength of 850nm, output power of 0.01W, operating voltage of 1.8 to 2.5V, operating current of 0.05 to 0.07A, output power (CW) of 0.01W.

2.2.1.2 L980P010

The L980P010 from Thorlabs Inc. is a LASER diode with a wavelength of 980nm, output power of 0.01W, operating voltage of 1.5 to 2.2V, operating current 0.025 to 0.04A, and output power (CW) of 0.01W.

2.2.1.3 L1270P5DFB

The L1270P5DFB from Thorlabs Inc. is a LASER diode with a wavelength of 1270nm, an output power of 0.01 W, an operating voltage of 1.1 to 1.6V, an operating current of 0.015 to 0.04A, an output power (CW) of 0.01W.

2.2.1.4 ML925B45F

The ML925B45F from Thorlabs Inc. is a LASER Diode with a wavelength of 1550nm, output power of 0.006 W, operating voltage of 1.1 to 1.5V, Operating Current of 0.010 to 0.05 A, output power (CW) of 0.006W.

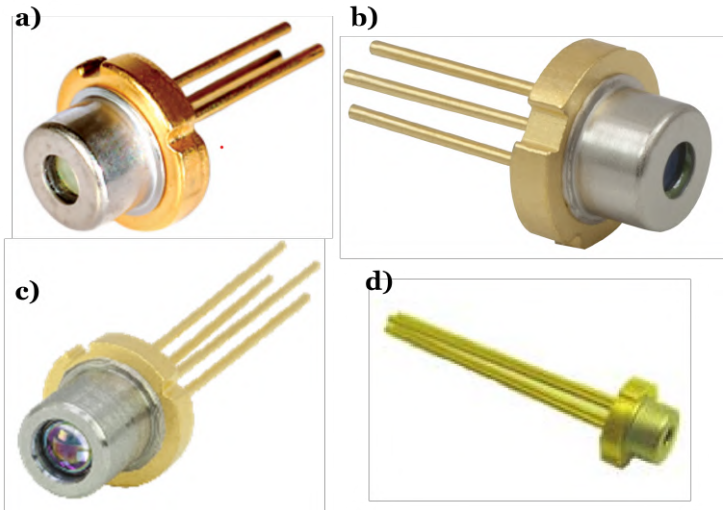

Figure 2.2: LASER Diodes: a) L850P010, b) L980P010, c)L1270P5DFB, and d) ML925B45F.

Benefits of using LASER Diodes as illumination source:

- Near-infrared light, emitted by LASER diodes, has excellent tissue penetration properties, allowing deeper imaging into breast tissues.
- This functional information provides insights into the biochemical and structural changes associated with breast cancer, aiding in early detection.

- LASER-based imaging techniques, combined with advanced data analysis, offer high sensitivity and specificity in detecting cancerous tissues.
- This technique does not require the use of ionizing radiation or the need for contrast agents, reducing patient discomfort and potential health risks.

2.2.2 Optic fiber channel

2.2.2.1 QR200-7-VIS-BX backscatter fiber probe

The reflection/backscatter probe, shown in figure 2.3, is a versatile and compact sampling option that allows for the measurement of diffuse and specular reflectance, and fluorescence from a wide range of samples, including solids, solutions, and powders. The probe assembly consists of low hydroxyl (Low OH) visible-NIR fibers, covering a wavelength range of 400-2100nm [26]. Valuable quantitative information about a sample's color, appearance, and chemical composition can be obtained using backscattered reflectance measurements.

The probe features a 6-around-1 fiber bundle design, where the 6-fiber leg connects to the light source, and the single-fiber leg attaches to the spectrometer. This design ensures efficient light transmission and accurate measurements.

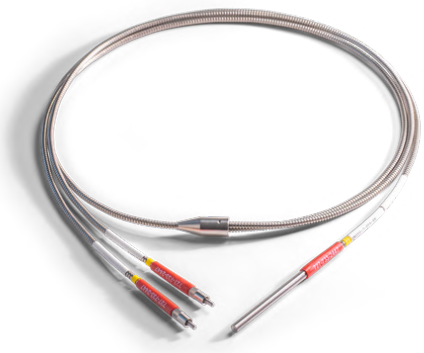

Figure 2.3: Reflection/backscatter probe [1].

Figure 2.4: Cross section view of probe [1].

2.2.2.2 BF44LS01 1-to-4 fan-out fiber optic bundle

The BF44LS01 is a 1-to-4 fan-out fiber optic bundle manufactured by Thorlabs. The optic fiber bundle has 400μm core diameter with low hydroxyl (Low OH) content, which makes it suitable for applications spanning visible to infrared wavelengths (400 - 2200nm). Each bundle consists of four multimode fibers with SMA905 connectors at both ends. The common end of the bundle is configured in a round arrangement, with a 1.05mm aperture and a fill factor of 58%

This fiber bundle is typically used in various optical and photonics applications where multiple fibers need to be routed from a single source. It has a total length of 1 meter and includes a common leg length of 0.25 meters.

Figure 2.5: BF44LS01 1-to-4 fan-out bundle.

2.2.3 Photodetector

2.2.3.1 PDAPC4

Figure 2.6: PDAPC4 InGaAs switchable gain photodetector, OEM package [2].

The PDAPC4 (shown in figure 2.6) is an OEM-packaged, amplified, switchable-gain photodetector made of Indium Gallium Arsenide (InGaAs). It operates within a wavelength range of 800 to 1700nm. The PDAPC4 comprises a reverse-biased PIN photodiode integrated with a switchable gain trans-impedance amplifier enclosed in a robust housing. The PDAPC4 includes a low noise, low offset, high gain trans-impedance amplifier that allows gain adjustment over a 70dB range.

The output voltage (V_o) from the photodetector is given by:

$$V_o = R(\lambda) \times G \times ScaleFactor \times P$$

Where,

V_o = Output Voltage from PDAPC4 in volts.

$R(\lambda)$ = Responsivity at wavelength (λ) in Ampere per Watts.

G = Trans-impedance gain for particular gain setting

P = Incident power on the PDAPC4 photodiode.

Scale Factor= 1 (for $R_{load} > 5$ KOhm).

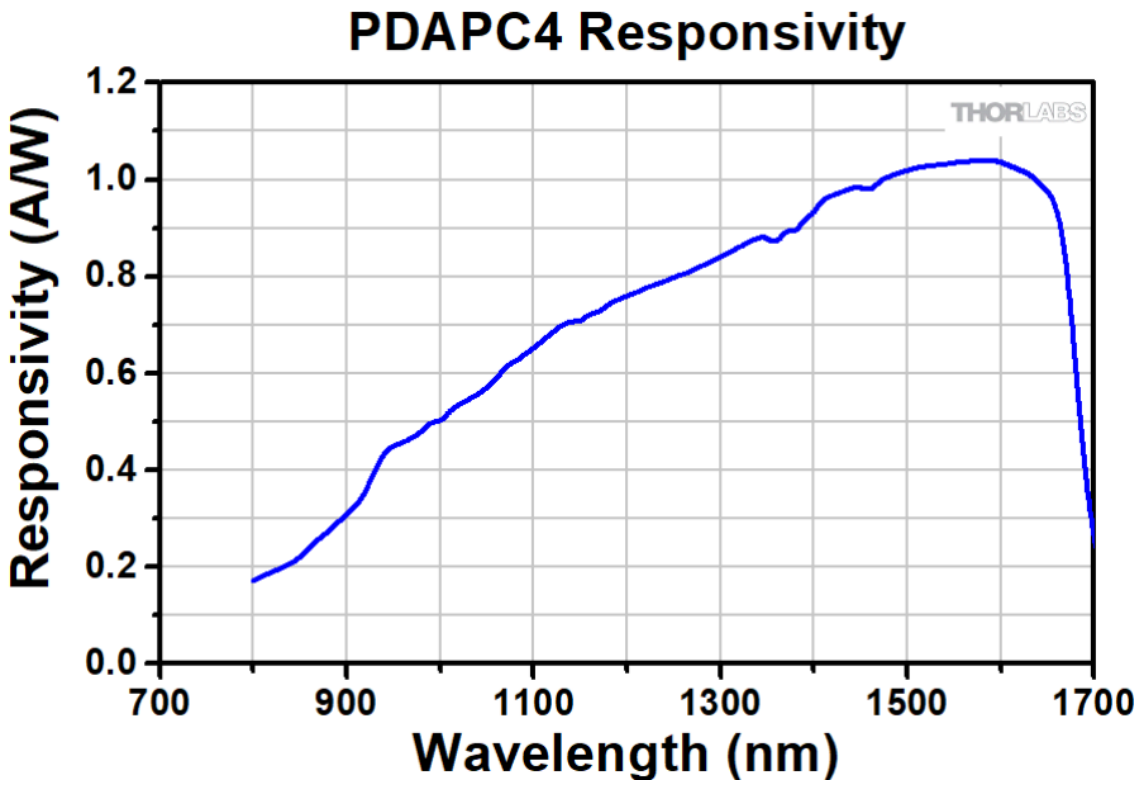

Figure 2.7: Response curve of PDAPC4 [2].

Max safe Operating Incident Power

The max power for PDAPC4 is limited by the saturation of the device's output amplifier. This will occur at 10V for HiZ termination measurements or 5V for 50 ohm termination (using 50 ohm serves as a 1/2 divider on the voltage output). The optical Power at which saturation will reach depends on the wavelength and related Responsivity in A/W for the photodiode. PDAPC4 has a peak response close to 1 A/W around 1550nm, though at 850nm the response is closer to 0.25A/W. This photocurrent flows into the amplifier where each gain setting has an associated V/A trans-impedance value. On higher gain settings, the detector will get saturated with less total optical Power. This saturation is just the condition of (photocurrent = power Watts * Responsivity A/W)*(gain in V/A) = (max output voltage, i.e. 10V for HiZ). A lower gain setting can be selected to reduce the gain; ND filters can be used to bring the Power below saturation or less LASER power can be applied to begin with to keep the output below the saturation voltage. For other wavelengths, corresponding responsivity for that wavelength is utilized, since this A/W value varies by a factor of 4x between 850nm and the peak response 1550nm. The gain is adjusted so that the measured signal level out of the PDAPC4 is below 10V (5V with a 50 ohm load) to avoid saturation.

2.2.3.2 Target specification

Table 2.1: Target specifications

1. Light source	Product Name	LASER diode
	Type Number	L850P010
	Storage temperature	-40 to 85 degrees
	Peak Wavelength	850nm
	Package	TO-18 can
	Operation Current	50mA
	LD Reverse Voltage (maximum)	2V
	Datasheet	https://www.thorlabs.com/thorproduct.cfm?partnumber=L850P010
2. Light source	Product Name	LASER diode
	Type Number	L980P010
	Storage temperature	-40 to 85 degrees
	Peak Wavelength	980nm
	Package	TO-18 can
	Operation Current	25mA
	LD Reverse Voltage (maximum)	2V
	Datasheet	https://www.thorlabs.com/thorproduct.cfm?partnumber=L980P010
3. Light source	Product Name	LASER diode
	Type Number	L1270P5DFB
	Storage temperature	-40 to 100 degrees
	Peak Wavelength	1270nm
	Package	TO Can with D pin code
	Operation Current	15mA
	LD Reverse Voltage (maximum)	2V
	Datasheet	https://www.thorlabs.com/thorproduct.cfm?partnumber=L1270P5DFB

4. Light source	Product Name	LASER diode
	Type Number	9xx45 SERIES 1550nm InGaAsP FP LASER DIODES
	Storage temperature	-40 to 85 degrees
	Peak Wavelength	1550nm
	Spectral width	3nm
	Operation Current	30mA
	LD Reverse Voltage (maximum)	1.5V
	Datasheet	http://www.princetel.com/datasheets/1550%20nm%20ML925B45F-01.pdf
5. Photodetector	Product Name	PDAPC4
	Detector	InGaAs
	Wavelength Range	800 to 1700nm
	Peak Wavelength	1590nm (Typ.)
	Peak Response	1.04A/W (Typ.)
	Amplifier GBP	600MHz
	Output Impedance	50Ω
	Max o/p Current	100mA
	Load Impedance	50Ω to Hi-Z
	Output Voltage	0 to 5V (50Ω) or 0 to 10 V (Hi-Z)
	Operating Temperature	10 to 40 °C
	Datasheet	https://www.thorlabs.com/drawings/87f56fca913d2887-14A95A8C-C981-8E66-5098AAD60929376C/PDAPC4-Manual.pdf

6. Fibre optic Probe	Product Name	Visible-NIR Reflection/Backscatter Probe
	Product No.	QR200-7-VIS-BX
	Wavelength Range Core size	400-2100nm 200μm / 400μm / 600μm
	Length	2m
	Jacket	PVDF zip tube, silicone-coated steel, mono coil Stainless steel BX
	Probe Ferrule Diameter	3.175mm or 6.35mm
	Datasheet	https://www.oceaninsight.com/products/fibers-and-probes/probes/reflectionbackscatter-probes/qr200-7-vis-bx/
7. SMA connector	Product Name	Amphenol 905 and 906 SMA Connectors
	Product No.	905-138-5002
	Cable type	Coaxial
	Impedance	50Ω
	Securing	Screw thread 1/4- 36 thread
	Maximum operating frequency range	0-18GHz
	Tightening method	Tightening method 8mm hex nut on male connector
	Datasheet	https://www.farnell.com/datasheets/1486544.pdf
8. Microcontroller	Product Name	Arduino ATMega2560
	Performance	16MHz
	Flash	256KB
	SRAM	8KB
	EEPROM	4KB
	Communication interfaces	8 UARTs, 4 SSI, 4 I2C, 2 CAN 2.0, USB2.0 OTG
	Maximum Supply Voltage	6-20V
	Maximum Output Current (per output pin)	50mA
	Datasheet	https://store.arduino.cc/products/arduino-mega-2560-rev3

Chapter 3

Design

The breast cancer diagnostic system's hardware design involves designing various modules and sub-modules. The key components include the ESS probe, which captures reflection from breast tissue, and the PCB responsible for efficient data acquisition and processing. Power supply module circuits are used to ensure the accuracy and reliability of the system. On the software side, modules consist of algorithms for data acquisition, processing, and creating a user-friendly GUI. Each module plays a crucial role in the smooth operation of the diagnostic system.

In the hardware design phase, rigorous designs for circuits are employed to address LASER diode and photodetector considerations. Then, the mathematical model [27], center-illuminated area detection (CIAD) to model the probe, is involved in integrating the ESS probe with the hardware and PCB. The design equations and the circuits form the foundation for selecting components and configuring the hardware to withstand the objective of developing a system for breast cancer diagnosis.

Industrial design aspects are carefully considered to optimize the breast cancer diagnostic system's physical appearance and user experience. The ESS data acquisition (DAQ) is designed for ergonomic handling and efficient data collection, while the PCB layout ensures compactness and functionality. Aesthetics are integrated into the overall design, ensuring that the system performs exceptionally and is user-friendly. Industrial design considerations focus on creating a product that meets technical requirements and aligns with user expectations and industry standards.

3.1 Module partitioning

Careful observation is given to component selection in the hardware design, comprising the ESS probe and the PCB. The choice of LASER diodes and the photodetector for the ESS probe, electronic components for the PCB, and their compatibility with performance specifications are critical decisions. Factors such as reliability, power consumption, and ease of integration are evaluated to ensure that the selected components align with the system's objectives and contribute to the effectiveness of the breast cancer diagnostic system.

Algorithms are the core of both hardware and software design. In the software domain, sophisticated algorithms are employed for data processing tasks, enabling the extraction of valuable information from the acquired reflectance. Algorithms are designed for data analysis, feature extraction, and decision-making processes crucial for breast cancer diagnosis. These algorithms are crafted with precision to enhance the sensitivity, specificity, and accuracy of the diagnostic system, contributing significantly to its overall performance.

3.2 Hardware design

The hardware design can be broadly divided into three parts based on the functionality of individual parts: source, channel (propagation medium), and detector.

3.2.1 Illumination source

The source consists of four LASER diodes of wavelength: 850nm, 980nm, 1270nm, and 1550nm. The significance of using LASER diodes is their characteristic property of generating a monochromatic, collimated beam of light, which has higher penetration depth and can be used to study highly selective effects of a given wavelength of light incident on the tissue. L850P010 [21], L980P010 [22], L1270P5DFB [23], and ML925B45F [24] are the LASER didoes from Thorlabs, Inc. used as illumination source with typical center wavelengths of 850nm, 980nm, 1270nm, and 1550nm, respectively. L850P010, L980P010, and L1270P5DFB have a maximum optical output power of 10mW, and ML925B45F has a maximum optical output power of 6mW. All the LASER diodes come in Θ5.6mm, TO Can package. L850P010, L980P010, L1270P5DFB and ML925B45F have maximum threshold current of 40mA, 25mA, 13mA, and 20mA respectively and operating current of 50mA, 25mA, 15mA, and 30mA respectively. Each LASER diode is coupled to one of the legs of the BF44LS01[28] fiber optic

bundles from Thorlabs, Inc., using SMA905 [29] connectors and in-house fabricated sockets. Each LASER diode is driven using an individual driver circuit, allowing independent control of each.

The LASER diode is in series with AL5809 constant current driver IC and N-channel logic level MOSFET with 5V supply voltage connected across the circuit, shown in figure 3.1. The typical operating voltage (V_{OP}) across L850P010, L980P010, L1270P5DFB and ML925B45F LASER diodes are 2V, 1.5V, 1.1V and 1.1V respectively. Due to the low $R_{DS_{on}}$ (∼4.8mohm) of MOSFET Q1, there is a very low drain to the source voltage drop (V_{DS} ∼72μV to 240μV) across the MOSFET. The remaining voltage (V_{DD}-V_{DS}-V_{OP}) drops across the AL5809 driver IC. AL5809 is a linear constant current driver with two pins. The operating voltage between the two terminals of AL5809 is between 2.5V and 60V, depending on the voltage drop across the LASER diode and MOSFET Q_1. AL5809 comes in different current ratings, providing different amounts of constant current in the circuit depending on the rated current. Our system requires 50mA, 25mA, 15mA, and 30mA constant current AL5809 driver IC for LASER diodes of 850nm, 980nm, 1270nm, and 1550nm, respectively.

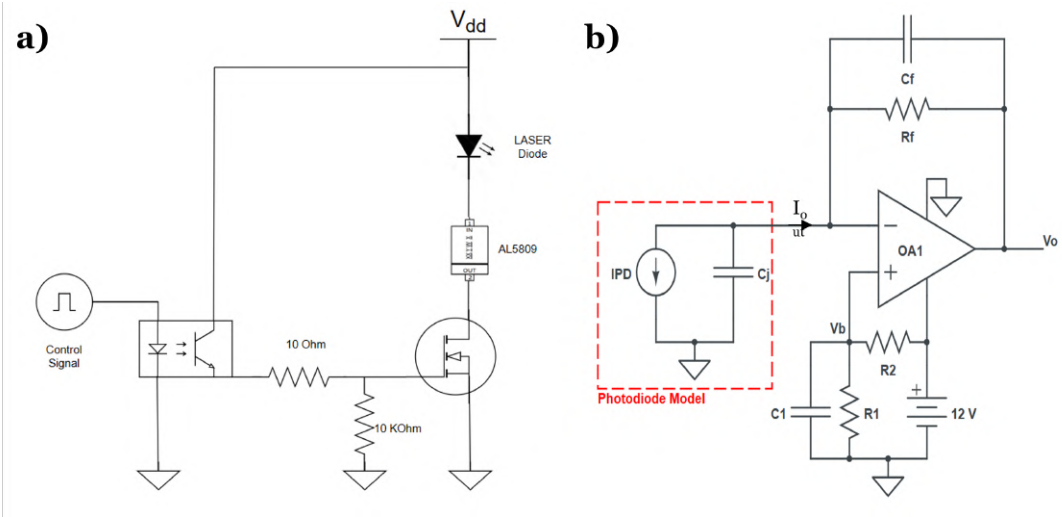

Figure 3.1: a) LASER diode circuit design, b) Monitoring photodiode circuit design.

The switching of LASER diodes is controlled by switching MOSFET Q1 with a typical gate-to-source threshold voltage of 1.8V and the Drain-to-Source Leakage Current of 1μA to 150μA, depending on the junction temperature. The control signal from the microcontroller actuates the light source inside the optocoupler, which emits light and activates the photodetector. The output end of the optocoupler starts conducting and introduces the supply voltage V_{DD} across the gate terminal, resulting in a gate voltage greater than the threshold voltage. This switches ON the MOSFET, and so the LASER diode. The optocoupler isolates the microcontroller

control pin from the external supply voltage V_{DD} to avoid damaging the controller unit. The significance of using external supply voltage V_{DD} is its driving capability to sufficiently charge the input capacitance of MOSFET Q_1, which is necessary for switching the MOSFET ON. The MOSFET gate resistor R1 helps suppress inrush current and reduces output ringing. A low-value register R_1 achieves a high switching speed, and a high-value register R_2 is used to bleed off the electric charge accumulated at the gate when M0SFET Q_1 is ON, reducing the gate-source voltage to 0V and turning off the MOSFET. The power dissipated by the MOSFET is I_{DS_2}*$R_{DS_{on}}$.

3.2.2 Optic fibre

Optic fibers are a propagation medium for effectively coupling light from source to detector. The light beam generated by the fiber-coupled LASER diodes propagates along the fiber and illuminates the region of interest in the ex vivo breast tissue. The backscattered diffusely reflected light is then collected using collection fiber, propagating the light to the fiber-coupled photodetector, shown in figure 3.2. The photodetector's output voltage measures the generated photodiode current, proportional to the incident power for a given wavelength. Two probes are utilized to establish a proper channel (or path) for the light generated from individual LASER diodes to incident on the breast tissue and to collect the backscattered light for detection at the photodetector side. The BF44LS01 is a 1-to-4 fan-out fiber optic bundle from Thorlabs with four high-grade multimode optical fibers in a round common end configuration on the other side of the cable. All ends of the bundle terminate with SMA905 connectors. BF44LS01 has four optic fibers FT400EMT, each with a core diameter of 400$\pm$ 8 μm and NA of 0.39 with an operating wavelength of 400 - 2200nm.

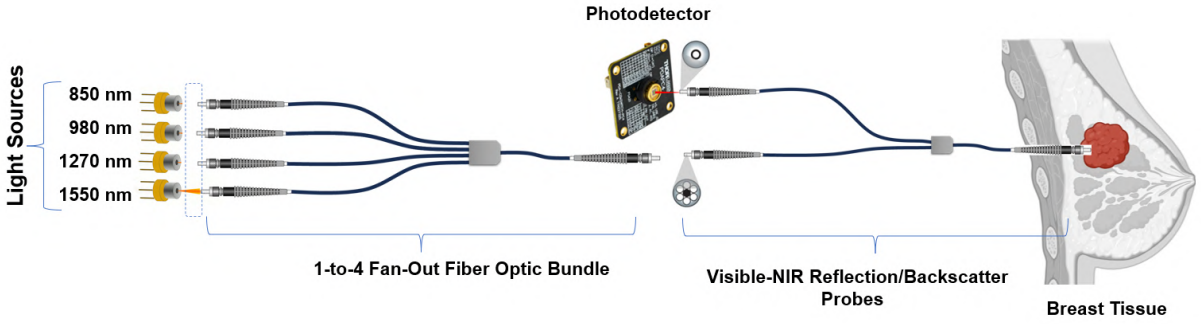

Figure 3.2: Visible-NIR probe is connected with BF44LS01 using SMA couplers.

Visible-NIR Reflection/Backscatter Probes, shown in 2.3, is a backscatter probe from Ocean

Insight, comprising visible-NIR multimode fibers (400-2100nm), each with a core diameter of 400μm. The probe has a 6-around-1 fiber bundle design at the end terminal used by the operator for illumination and collection of the light from the tissue sample. The other side consists of two optic fiber legs: one with six fibers in a circular arrangement for illumination and the other having a single fiber at the center for collecting the backscattered light from the sample. The backscatter fiber optic probes are insensitive to noise due to light from the illumination source; hence, they best suit our application. The disadvantage of the backscatter configuration is that the amount of optical power reaching the receiver is lower than that of the forward configuration. This is because scattering in breast tissue is highly forward-directed with a g value. This can be compensated by improving the signal-to-noise ratio at the receiver end.

Three types of coupling present in our system collectively build the channel for light propagation. These are 1) source-to-fiber coupling between the four LASER diodes and four individual legs of 1-to-4 fan-out fiber optic bundles with a single fiber in each leg. 2) fiber-to-fiber coupling between the common round end of 1-to-4 fan-out fiber optic bundles and six fiber legs of Visible-NIR Reflection/Backscatter Probe. 3) Fiber-to-detector coupling between the single-fiber leg of the Visible-NIR Reflection/Backscatter Probe and PDAPC4 photodetector. Light attenuates while it propagates through the optic fiber channel. The attenuation is mostly due to the coupling losses at different coupling ends. Total coupling losses in the system are the sum of coupling losses at source-to-fiber, fiber-to-fiber, and fiber-to-detector coupling. Source-to-fiber coupling losses are due to the divergent nature of the light emerging from the LASER diode.

3.2.3 Photodetector

The backscattered reflected light is detected using an Indium Gallium Arsenide (InGaAs) based photodetector (PDAPC4) from Thorlabs [25], sensitive to near-infrared light (800 to 1700nm). PDAPC4 is an amplified photodetector with a built-in low-noise trans-impedance amplifier. The gain can be varied in 10dB steps using the DIP switch given or through programmable pins. The maximum output of the PDAPC4 is 10V for a high impendence load (RL $\geq$ 5 Kohm), and the gain is adjusted such that the measured signal voltage from the PDAPC4 output is below 10V to avoid saturation. The output voltage from PDAPC4 is:

Output Voltage (V) = Responsivity (A/W) $\times$ Transimpedance Gain (V/A) $\times$ Scale Factor $\times$ Input Power (W)

where,

Photocurrent Generated (I_{PD}) = Responsivity (R(λ)) $\times$ Incident Light Power (P_I)

Output current (I_o) = dark current (I_{dark}) + Photodiode current (I_{pd})

The photodetector circuit is designed in such a way that it manages to have a very low dark current, and hence it can be neglected, which means,

Output current (I_o) = Photodiode current (I_{PD}) = Responsivity (R(λ)) $\times$ Incident Light Power (P)

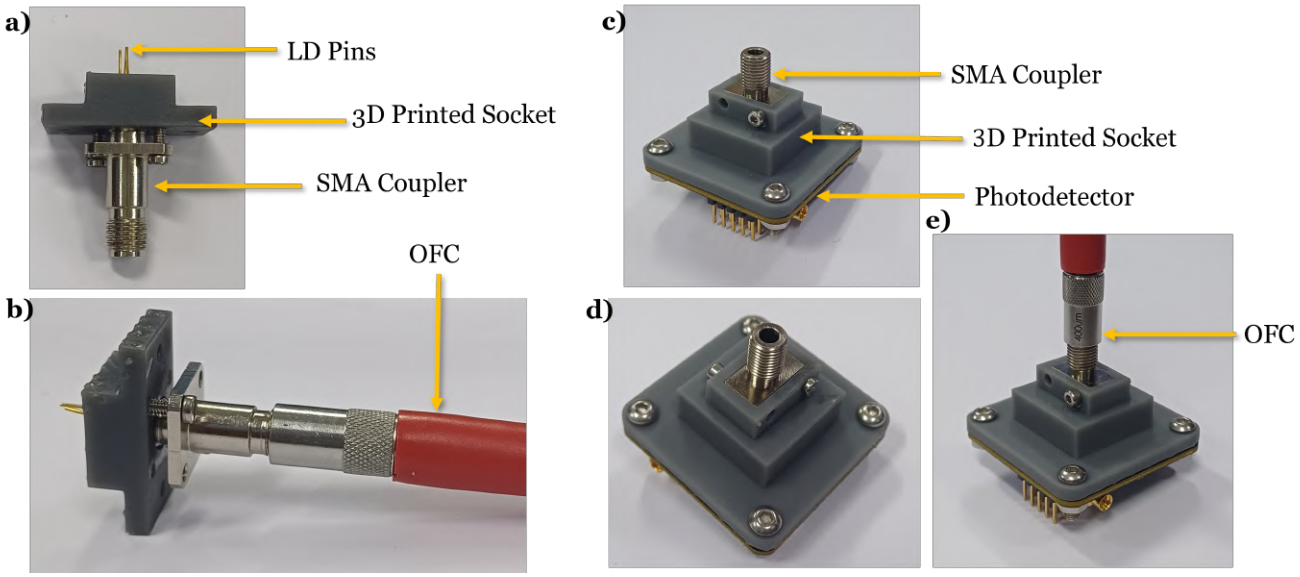

Figure 3.3: a) LD with 3D printed socket and SMA coupler, b) LD coupled to optic fibre cable, c) PD with 3D printed socket and SMA coupler, d) Isometric view of PD, and e) PD coupled to optic fiber cable.

The PDAPC4 gives out analog voltage as output, which, after digitization using a 16-bit ADC ADS1115 [30], is given to the microcontroller, which forwards the reading to the computer for further processing. The ADS1115 ADC has a resolution of 76uV compared to the inbuilt ADC in the microcontroller with a resolution of 4.9mV. The ADS1115 module communicates with the microcontroller using the I2C communication protocol. The PDAPC4 is coupled to the detector leg of the visible-NIR reflection/backscatter probes using a SMA905 connector and an in-house fabricated socket, as shown in figure 3.3. The EC4PS (Model #: ECM100UT31) power supply module from Thorlabs with the output voltage of +5 V \ $\pm$12 V and output power of 75W provides supply voltages of +12V, -12V, and ground, required for the proper working

of the data acquisition module.

3.3 Software design

This section explains about the details of the software components crucial to the functionality of the breast cancer diagnostic system. The software design encompasses the embedded software responsible for data processing on the hardware front and the graphical user interface (GUI), which serves as the user's portal to interact with the system.

The development of effective software GUIs is essential, as are precision, reliability, and user-friendliness. The GUI operates critical data processing tasks, extracting valuable information from the elastic scattering spectroscopy (ESS) probe. Simultaneously, the GUI provides an intuitive interface, facilitating communication between the user and the data acquisition system.

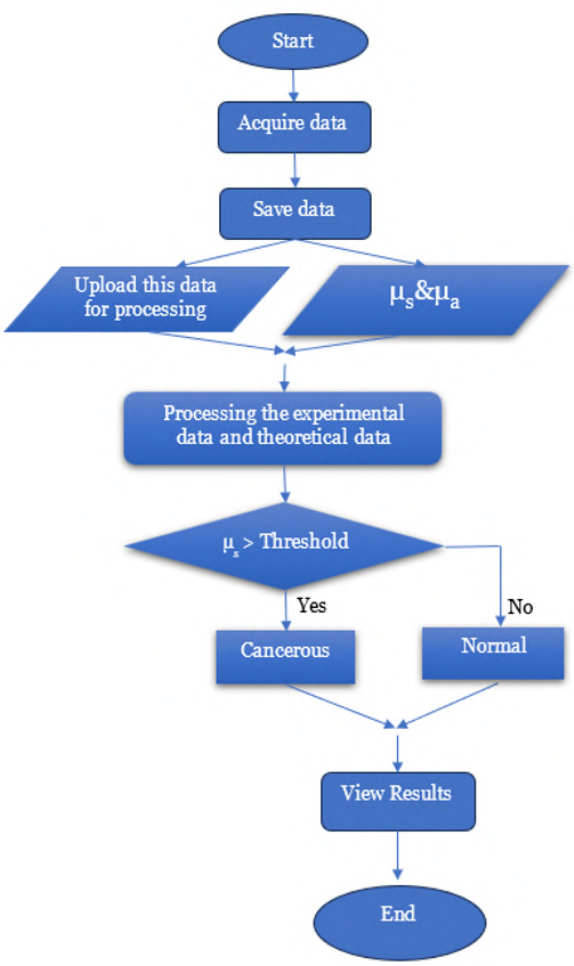

Figure 3.4: Process flow for data acquisition and processing.

Table creation and dynamic management: This module is responsible for creating and managing the dynamic table used to display the acquired data. Implemented using HTML templates and Flask, the table structure is dynamically generated based on the start button's click. The Flask server handles requests for adding or deleting rows, simulating real-time data acquisition events. Pandas, a Python data manipulation library, manages and manipulates the server dataset efficiently.

Integration of button modules:

- **Start button**: The "Start" button serves as the beginning for data acquisition, triggering the commencement of the experimental process. Employing an 'on click' event in HTML, this button connects with underlying JavaScript functions to initiate systematic data gathering.
- **Save button**: The "Save" button is pivotal in data management. This button preserves datasets with a single click; users can store information, ensuring that collected data are securely archived and readily accessible for subsequent analyses.
- **Calibrate button**: The "Calibrate" button allows users to fine-tune system parameters dynamically. Leveraging JavaScript functions enables users to adjust and optimize the system for enhanced performance. This feature allows users to adapt the system to specific experimental requirements, ensuring precision and accuracy in data collection.
- **View results**: The "View Results" button transforms raw data into visually appealing and comprehensible graphical representations using Matplotlib and Searborn libraries. Upon activation, this button dynamically generates graphs, offering users an insightful visualization of the experiment's outcomes. The seamless incorporation of these libraries enhances the user interface, providing a clear and intuitive interpretation of the results.
- **Delete button**: The "Delete" button facilitates the removal of redundant or undesired data points. Its implementation ensures that users have control and eliminate data entries that are not required. This feature helps acquire correct data with high accuracy and precision, empowering users to maintain a well-curated dataset.
- **Metrics button**: The "Metrics" button is a gateway to comprehensive performance insights. It provides a detailed overview of system metrics. These include key performance indicators, statistical analyses, and other relevant metrics. The integration of advanced algorithms ensures the delivery of accurate and meaningful metrics, enhancing the system's overall utility.

Data visulaization in graphical representation: Upon activation of the ”View Results” button, an interplay of the Matplotlib and Seaborn libraries translates the raw data into interpretable graphs. The button triggers a rendering process that transforms the dataset into intuitive graphical representations. The incorporation of Matplotlib ensures the generation of high-quality, publication-ready plots, while Seaborn enhances visual aesthetics and statistical insights. Furthermore, a feature allows users to delve deeper into the details by hovering over specific data points on the graph. This responsive zoom functionality, implemented through JavaScript, empowers users to magnify and scrutinize specific regions of interest, providing a granular perspective on the plotted data. This interactive graphing facilitates the exploration of experimental outcomes, fostering a deeper understanding of the underlying patterns and trends within the data.

3.4 Industrial design

Each part has been meticulously engineered in industrial design to achieve high technical proficiency and user-centric functionality. As shown in figure 3.6, the enclosure is a culmination of precision engineering, illustrated in 3.5, considering the optimal placement of the PCB and power modules by utilizing a step file generated from Altium. It ensures integration that aligns with functional requirements. The front panel is not merely an aesthetic element but also a strategic interface designed carefully considering user ergonomics, such that LASER diodes and PDAPC4 are coupled to a PCB. Its layout is mapped to house controls that facilitate efficient user interactions, creating a tactile and intuitive experience.

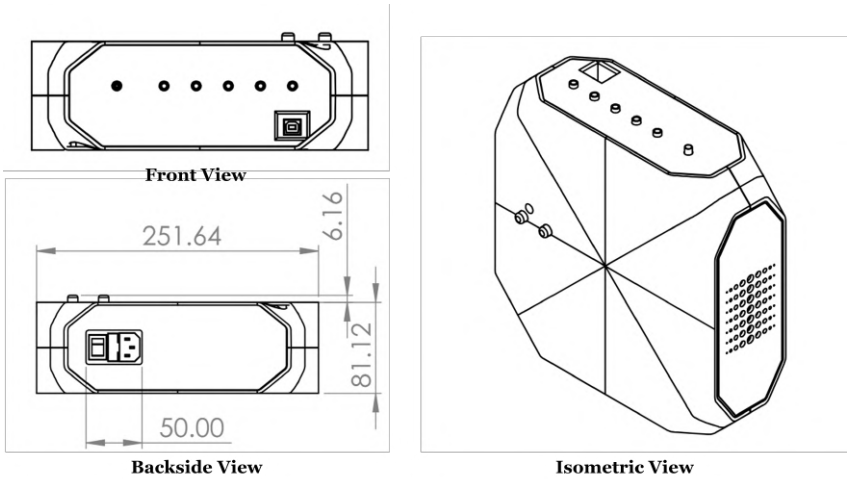

Figure 3.5: Engineering drawings of the 3D case.

A cooling fan has been integrated to dissipate heat efficiently, ensuring the optimal performance and longevity of the components. The power switch, positioned for accessibility, adds an extra layer of user control, allowing for convenient on/off functionality.

The placement of buttons extending from the PCB to the 3D model has been extended. This design serves a practical purpose, providing users with direct access to key functionalities. The buttons are positioned for ergonomic ease, promoting intuitive operation while maintaining a visually cohesive front panel. The glow from the LEDs adds a visual cue, enhancing the user interface and providing immediate feedback on the system's operational state. The Altium-generated step file for the PCB adds an additional layer of technical precision. This enables the integration of the PCB into the overall design, ensuring that electrical components are placed with the utmost accuracy. This technique extends to the placement of components, offering a comprehensive understanding of the internal architecture. Industrial design is a testament to the fusion of technical ingenuity, user-centric considerations, and meticulous attention to detail.

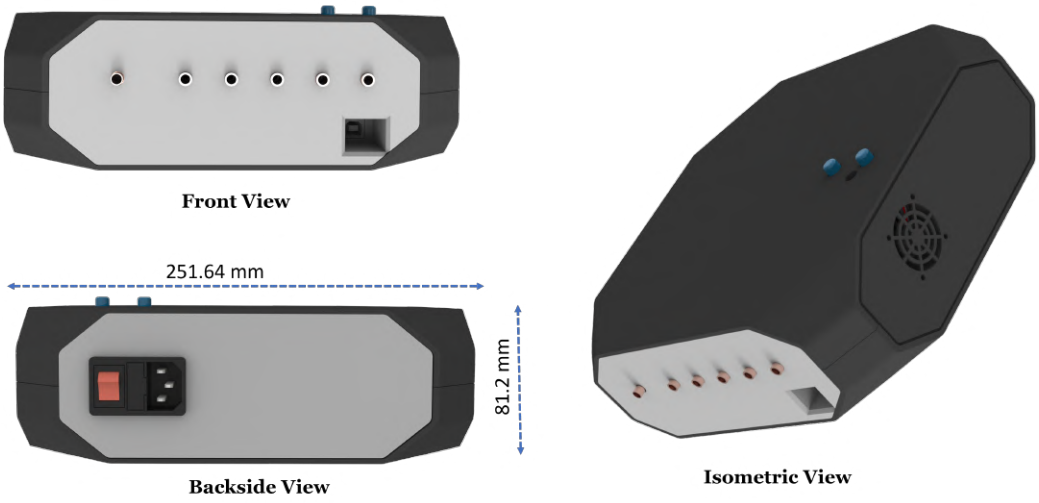

Figure 3.6: 3D-Printed casing of data acquisition system.

Chapter 4

Engineering

4.1 Product structure

A novel, robust, real-time, and user-friendly diagnostic system is developed to delineate the cancerous breast tissue from adjacent normal tissues. The system is based on the principle of elastic scattering spectroscopy. Due to the heterogeneous nature of breast tissue, incidence photons spread in different directions, resulting in scattering of light. An optical probe is used to collect these backpropagated scattered light, and then the perturbation in light is sensed by the photodiode. Sizes, refractive indices, and structures of the subcellular components (e.g., nucleus, nucleolus, and mitochondria) are known to change when cells become malignant. Thus, the optical properties of healthy and diseased tissues differ; this enables the determination of the disease state of the tissue.

4.2 Hardware modules

4.2.1 Printed circuit board (PCB)

4.2.1.1 PCB schematic

The Altium Design software provides the ease of use of the design methodology for the desired PCB; the schematic diagrams serve as the foundation of our breast cancer diagnosis system. A schematic diagram illustrates the involved electrical connections and component placements, which are essential for functionality. The schematic is built using Altium's interface, providing

a comprehensive overview of the circuitry and enabling precise design and analysis. The developed system comprises several modules present in the schematic such as a Voltage regulator, power supply, Arduino microcontroller, LEDs, LASER Diodes, and connectors.

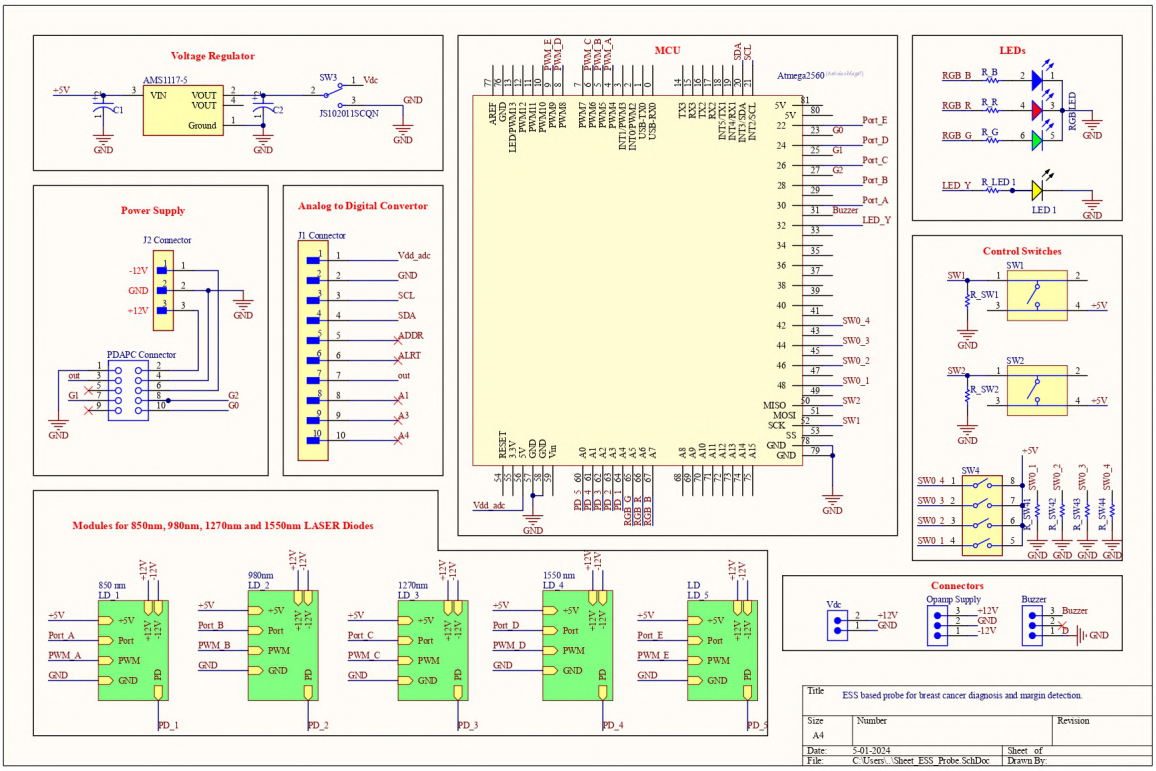

Figure 4.1: PCB schematic of data acquisition (DAQ) System.

4.2.1.2 PCB layout and routing

Utilizing Altium Designer Software's advanced layout and routing capabilities, the PCB design is crafted to optimize space utilization and minimize interference. PCB layout gives the blueprint that can guide the designer for the production of circuit boards, which lays the foundation for the development of the system. The software's powerful routing tools enable the creation of efficient trace paths, while the layout features facilitate component placement, ensuring robust electrical performance and reliability.

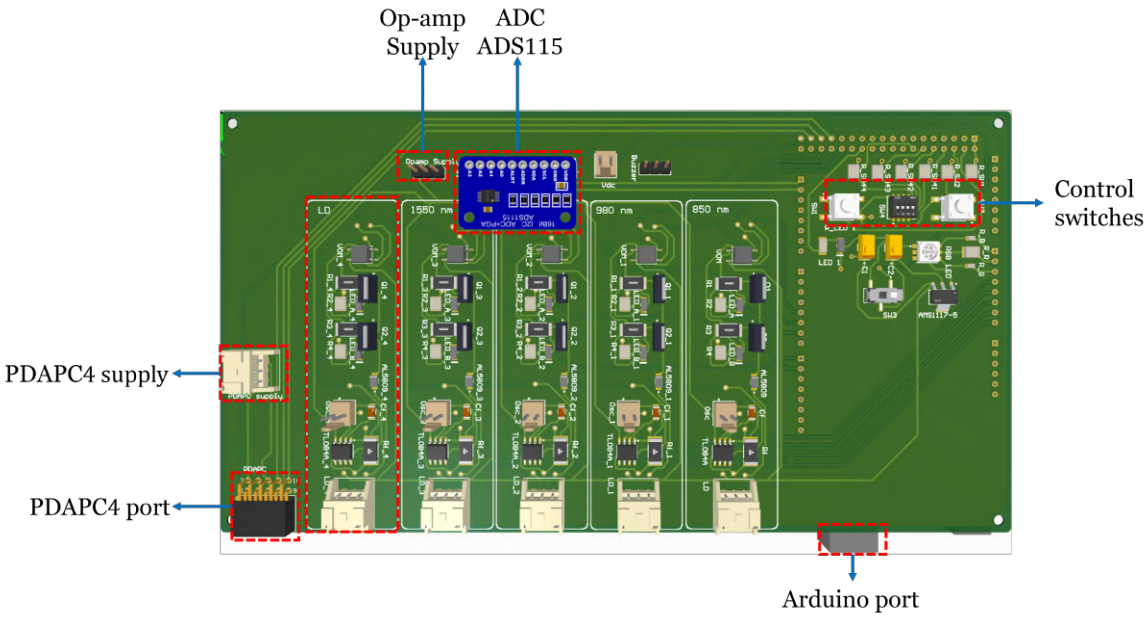

Figure 4.2: PCB layout top-view.

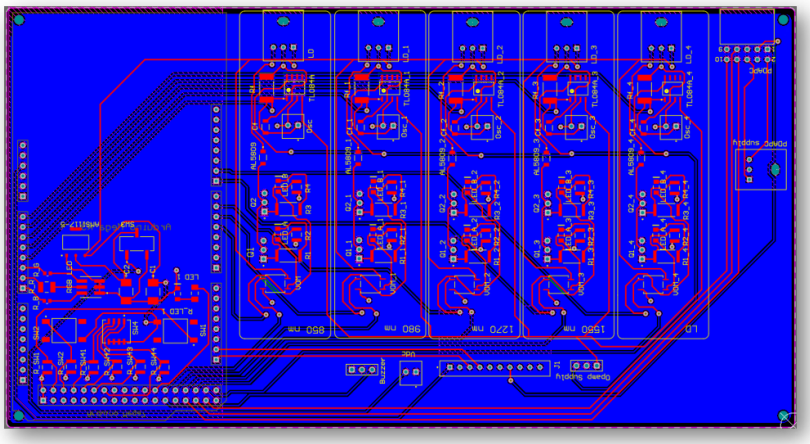

Figure 4.3: PCB routing.

4.2.1.3 PCB assembly

Altium Designer streamlines the PCB assembly process, allowing for the integration of components and efficient manufacturing workflows. The solder paste is utlilized for mounting the Surface Mount Device (SMD) Components. Pin-hole components are soldered using a soldering iron rod. With Altium's assembly features, component libraries, and design rule checks, the reliability and performance of the final product are achieved.

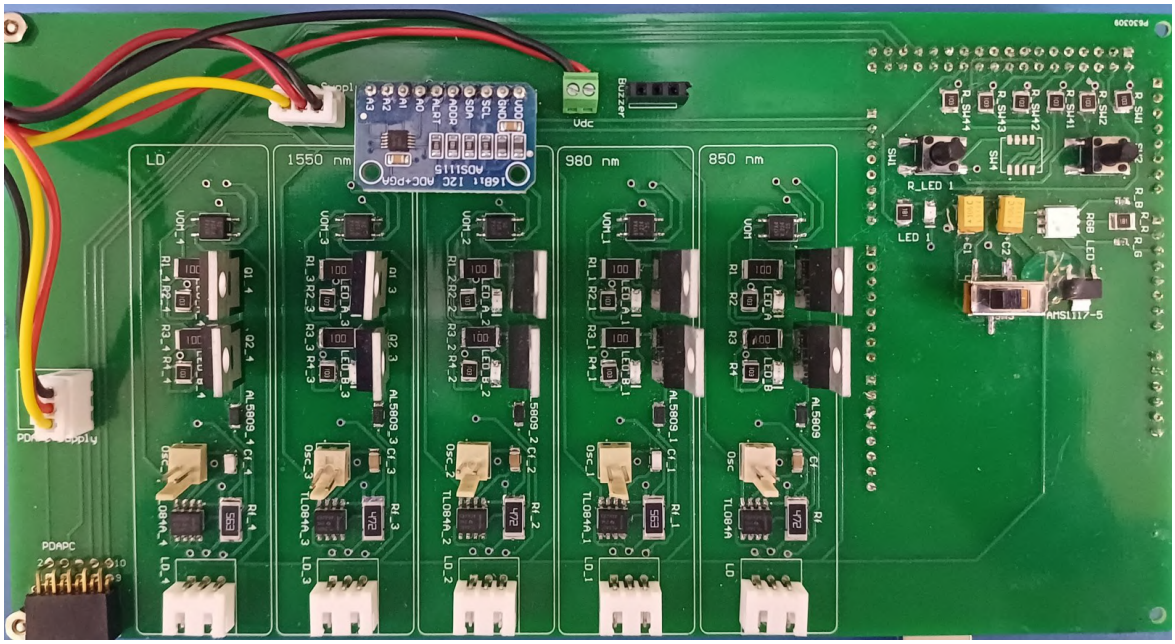

Figure 4.4: Actual image of PCB after mounting the components.

4.2.2 3D-case enclosure for the system

A probe system is developed through 3D printing that is used for positioning the PCB and power adapter so that the Arduino connector port is provisioned towards the right corner and the LASER diodes outlets on the front, shown in figure 4.5. The list of components that connect to the system is listed in the table 4.2.2.

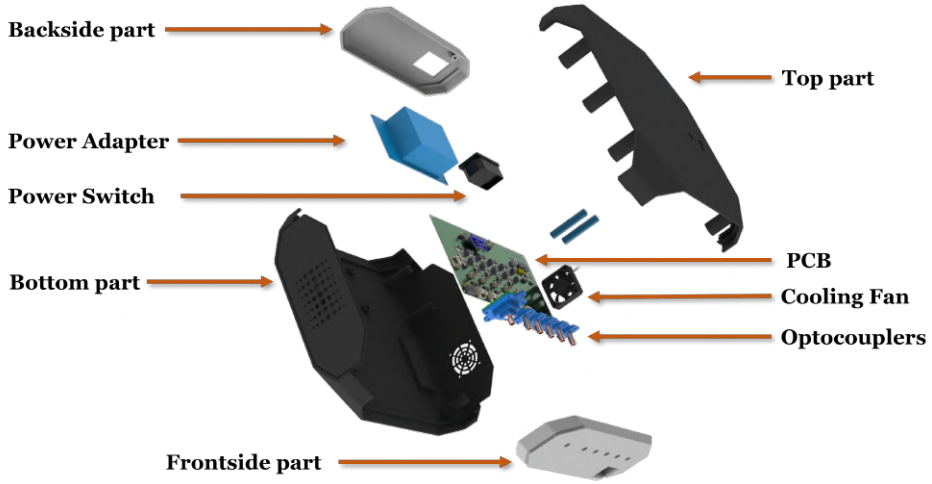

Figure 4.5: Scattered view of 3D-printed casing of DAQ system.

Table 4.1: List of hardware components

S.No	Component	Qty	Description	Vendor	Price(INR)
1	BF44LS01-1 to 4 Fan out Bundle	1	1to4 Fan-Out Bundle, 400μm Core, Low OH, SMA, Round Common End, 1 m Long	Thorlabs	38758.22
2	EC4PS - Power Supply Module	1	100W, +5V \ $\pm$12 V Power Supply Module for Custom Electronics Assemblies	Thorlabs	20414.73
3	PDAPC4 - Switchable Gain Photodetector	1	InGaAs Switchable Gain Detector on PCB, 800 - 1700nm, 11MHz, 3.14 mm	Thorlabs	25596.55
4	L850P010-850nm LASER Diode	1	850nm, 10 mW, ϕ5.6mm, A Pin Code, LASER Diode	Thorlabs	2269.68
5	L980P010-980nm LASER Diode	1	980 nm, 10 mW,ϕ5.6 mm, A Pin Code, LASER Diode	Thorlabs	2626.88
6	L1270P5DFB-1270nm LASER Diode	1	1270 nm, 5 mW, ϕ5.6 mm, D Pin Code, DFB LASER Diode	Thorlabs	20414.73
7	ML925B45F-1550nm LASER Diode	1	1550 nm, 5 mW, ϕ5.6 mm, D Pin Code, LASER Diode	Thorlabs	4764.72
8	Arduino Mega 2560	1	Mega 2560 ATmega2560-16AU Board for Arduino	Sharvi Electronics	1342.56
9	Visible-NIR fibers probe	1	Part Number: QR200-7-VIS-BX	Oceaninsight	2626.88
10	SMA couplers	6	Fiber Adapter Square type Fibre Connector SMA905/906 Coupler	Ebay	1156.75

11	Cooling fan	1	Sunon 4010 5VDC 0.83W Cooling Fan	Robu	299
12	Power Cord	1	1.2M AC 10A 250V Power Supply Cable EU Plug	Robu	88
13	LASORB L44-47-122-208-X	5	LASORB ESD Absorber for LASER Diode	Pangolin LASER Systems	3130.25
14	LASORB L44-47-121-392-X	2	LASORB ESD Absorber for LASER Diode	Pangolin LASER Systems	1252.1

4.3 Software modules

In the engineering phase, attention is given to every aspect of the software modules, ensuring functionality and efficiency. Each module follows a comprehensive development cycle, incorporating the following key elements.

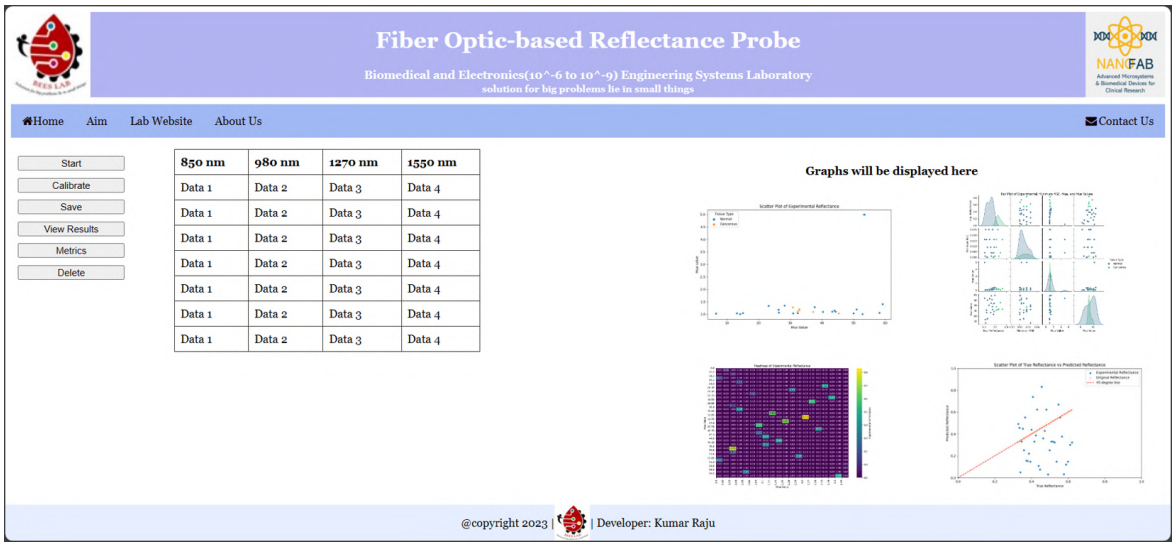

Figure 4.6: GUI front panel.

The software module we are testing is a key part of our larger system. This module details the steps in creating, using, and testing the GUI. Each part of the GUI, from the setup details and algorithmic design to compilation processes and testing procedures, is meticulously developed to present a comprehensive understanding of the module's engineering architecture.

The LASER Diode illumination is divided upon a unit time into four parts where each LASER diode is ON respectively, as shown in figure 4.7.

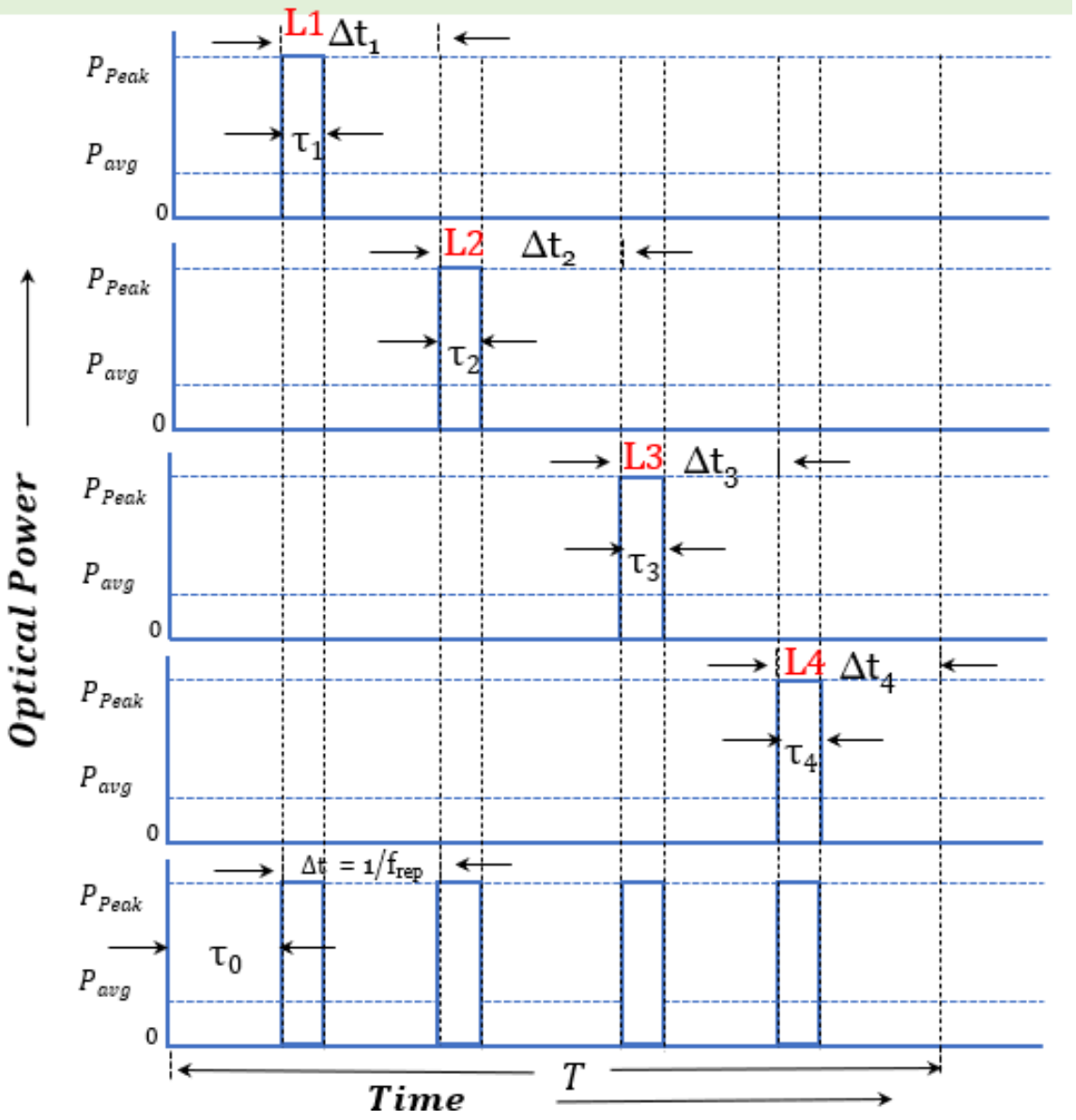

Figure 4.7: Data acquisition cycle.

4.4 Mathematical model

ESS identifies the tissue medium's bulk optical properties, including absorption and scattering coefficients, obtained by light remission after intra-medium propagation. There are two aspects required for ESS: firstly, a probe for probing the desired tissue, and secondly, a model of light-tissue interaction pertinent to the probing geometry. The interdependence of the aspects and the absence of a precise analytical solution for light-tissue interaction motivated me to develop a more accurate, resilient, and user-friendly mathematical model. Among the many configurations, single-fibre reflectance (SfR) [27] is easy to understand and implement. The complexity of determining the diffuse reflectance for SfR has been alleviated by utilizing a single integration method weighted by a probability distribution function (PDF). The diffuse photon remission collected using the single-fiber geometry scales the total diffuse reflectance over the same location under centered illumination, and a model is reported. The characteristic of simple scaling between SfR and center-illuminated-area-detection (CIAD) geometries eases the complexity of a single-integration model for SfR while leveraging the advantages of the PDF. The collecting fibers encircle a center-illuminating fiber, or illuminating fibers surround a center-collection fiber. The diffuse reflectance resolved radially at a distance ρ from the point of interest (POI) is represented as R(eq. 4.1). The radially resolved diffuse reflectance within the inner region depends on the parameter g. The diffuse reflectance for CIAD geometry is obtained analytically by integrating the area under the radially resolved photon remission resulting from illumination at the center.

$$\boxed{R = \frac{0.75^g}{2\pi} 10^{-(1+p_1\gamma)} \frac{\mu_s^2 (1-g)^g}{\mu_s \rho^{(1+\gamma)}} exp(-\gamma)} \tag{4.1}$$

where $\gamma = 2\frac{\mu_a}{\mu_s}$, $p_1 = 1.25, \rho = 0.4mm, g = 0.9$

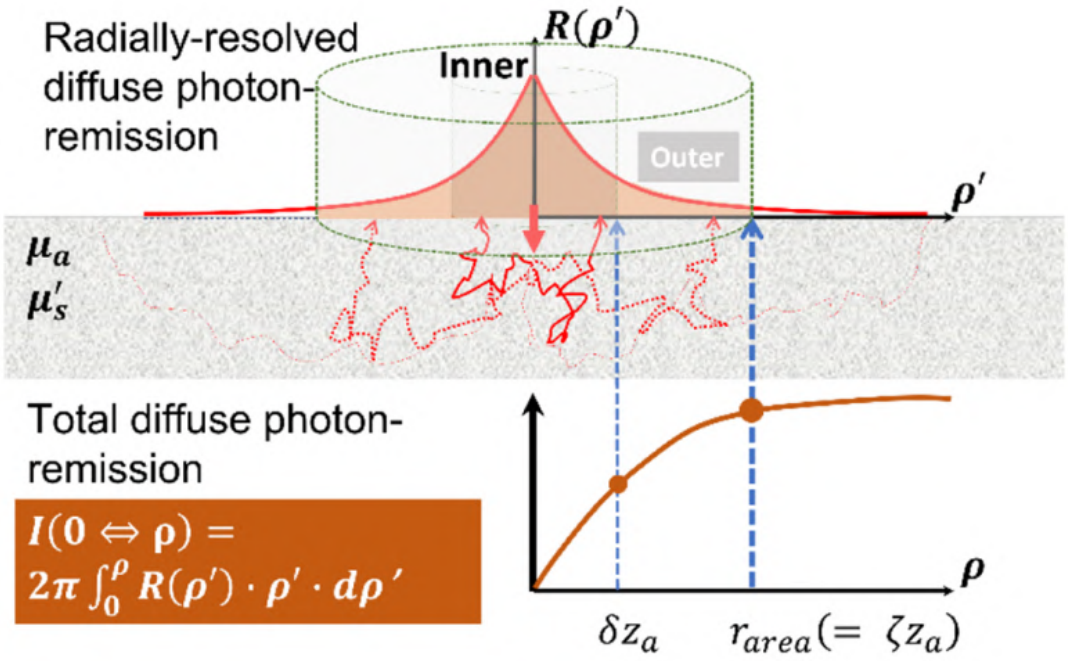

Figure 4.8: Mathematical modeling: Geometry of concern of the probe.

4.5 Experimental setup

The setup is arranged on a bench for laboratory use, keeping the data acquisition (DAQ) system in an electro-static discharge (ESD) free place to avoid sudden surge spikes for LASER Diodes in the developed system. Then, power the probe system and arrange the formalin-fixed tissues for experiments. After that, place the probe on the *ex-vivo* tissue and acquire the data using GUI. The complete table setup of the system is shown in the figure 4.9. The patient's written consent was obtained per the protocol submitted to the institutional ethics committee of the Indian Institute of Science and Assam Medical College, bearing ethical clearance certificate numbers 17-14012020 and AMC/EC/311, respectively.

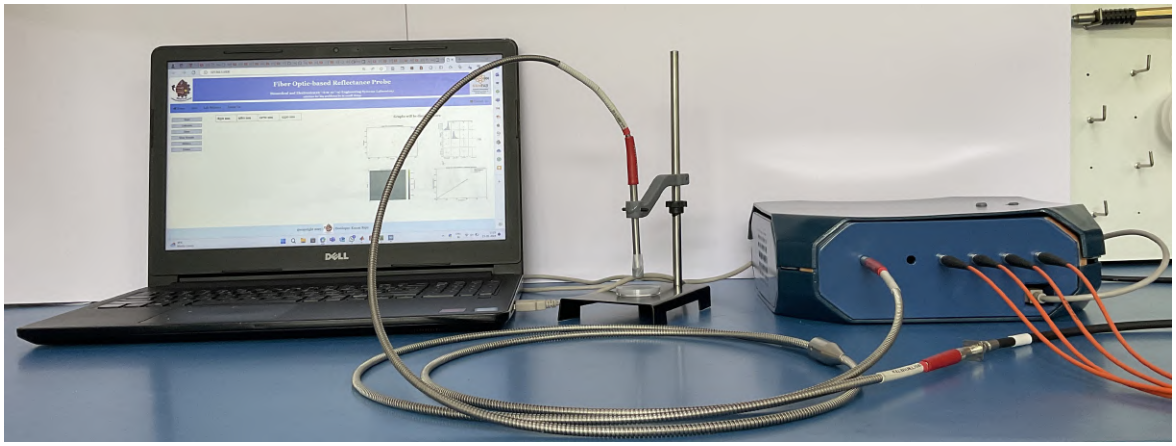

Figure 4.9: Experimenteal bench setup of the system.

The probe tip is placed on the phantom to measure the reflectance standard. After that, the probe is shifted to *ex-vivo* breast tissue, as shown in the figure 4.10.

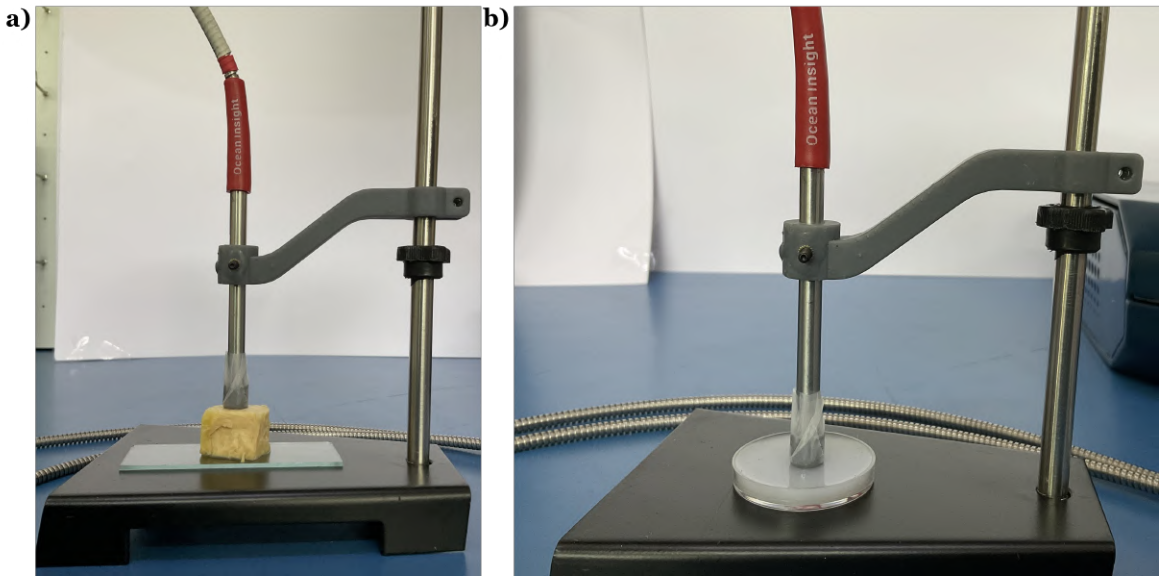

Figure 4.10: (a) Probe tip on *ex-vivo* tissue (b) Probe tip on phantom.

The experiment is then carried out on a big lump of breast tissue; a grid-structured 3-D shape is utilized to place the probe tip on the tissue for uniformity in acquiring the data, as shown in figure 4.11.

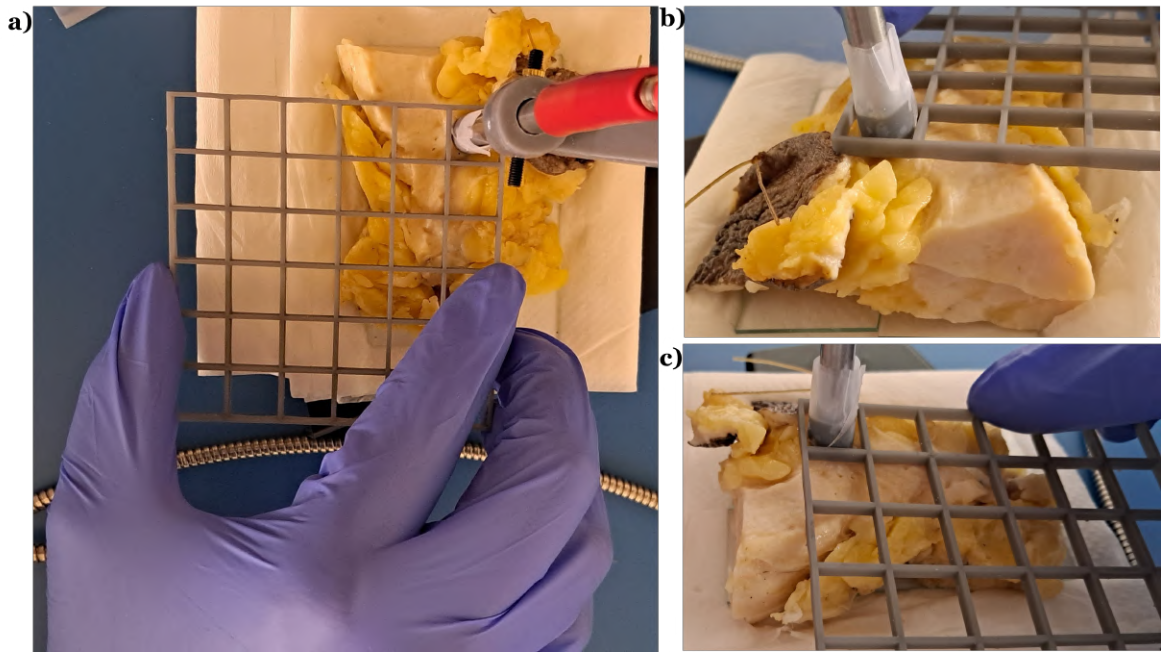

Figure 4.11: Reflectance measurements of *ex-vivo* tissues: a) Top-view, b) Side-view, and c) Isometric-view.

The absolute reflectance of breast tissue sample is given by:

$$R_{tissue} = \frac{I_{refelected}}{I_{incident}} \tag{4.2}$$

Where,

$I_{reflected}$ = Reflected radiation intensity from "infinite thick" tissue sample.

$I_{incident}$ = Intensity of incident beam.

As calculating $I_{incident}$ is practically difficult. The relative reflectance measurements for the tissue is used and is given by:

$$R'_{tissue} = \frac{R_{tissue}}{R_{standard}} \tag{4.3}$$

Where,

R_{tissue} = Absolute reflectance of the breast tissue sample.

$R_{standard}$ = Absolute reflectance of the reflectance standard ($BaSO_4$).

This relative reflectance is then related with the output voltage from the photodetector using equation:

$$\boxed{R'_{tissue} = \frac{R_{tissue}}{R_{standard}} = \frac{P_{tissue}}{P_{standard}} = \frac{V_{tissue}}{V_{standard}}} \tag{4.4}$$

Where,

P_{tissue} = Reflected radiation power from the tissue sample.

$P_{standard}$ = Reflected radiation power from the reflectance standard ($BaSO_4$).
V_{tissue} = Output voltage when reflected radiation from the tissue sample is incident on the photodiode.
$V_{standard}$ = Output voltage when reflected radiation from the reflectance standard is incident on the photodiode.

4.6 Phantom preparation and recipe

Polydimethylsiloxane (PDMS) [3], composed of silicone, is used for crafting tissue-mimicking phantoms due to its excellent processability, durability, noncytotoxic, non-flammable, and biocompatibility flexibility, and adept at optical, mechanical, and thermal properties. PDMS-based phantoms can be adjusted for a wide range of optical properties across the visible to near-infrared spectrum. Biological tissues' absorption and scattering coefficients depend on the no. of photons absorbed (or) scattered per centimeter of tissue. PDMS is utilized to create phantoms that mimic biological tissues' optical, physical, and thermal characteristics. At room temperature, PDMS is fluid, but its properties can be modified by mixing curing agents such as methyl hydrogenated silica, dimethyl vinylated silica, or trimethylated silica. PDMS molecules gradually undergo polymerization and transform the fluid into an elastomer within several hours to days. Polymerization allows PDMS to emulate Young's modulus (approximately 0.1 to 1 MPa) characteristic of soft tissues. Tissues such as the breast, cartilage, kidney, and stomach possess refractive indices ranging from 1.4 to 1.5 at visible wavelengths. The refractive index of PDMS can be adjusted from 1.405 to 1.445 by altering the curing temperature or the proportions of the curing agents. Light-absorbing agents like Indian ink, nigrosine dye, and coffee are utilized to modify the absorption coefficient of PDMS phantoms. Scatterering agents like TiO_2 and AlO_2 particles adjust the scattering coefficient.

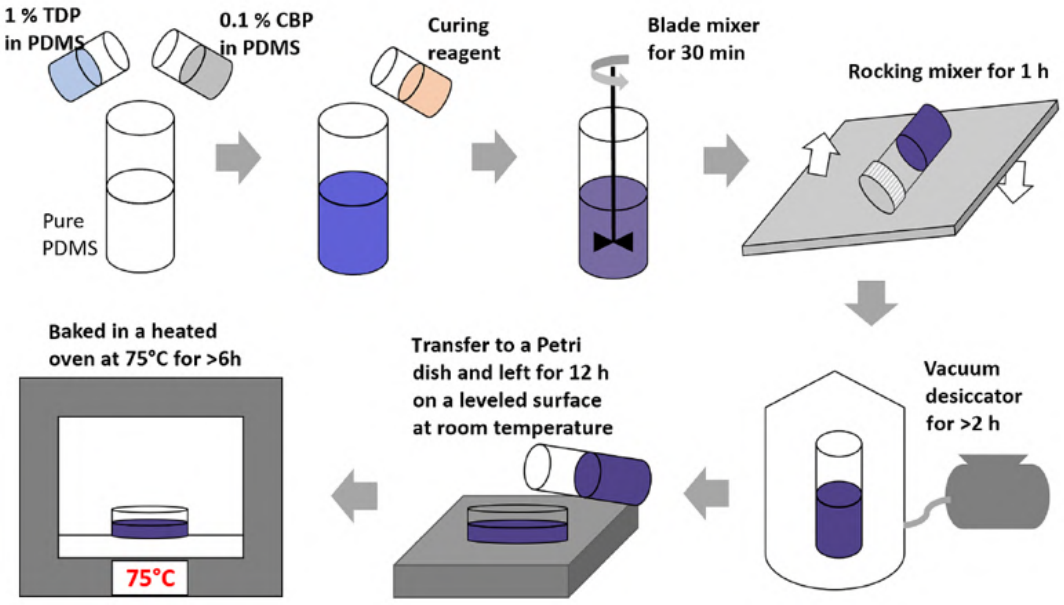

Figure 4.12: Process flow for the phantom fabrication [3].

PDMS-based phantoms containing scattering agent titanium dioxide particles (TDP) and absorbing agent India Ink spread within the PDMS. Initially, two distinct suspensions of PDMS are prepared: one constitutes dispersed TDP (1% TDP in pure PDMS, w/w ratio), and the other contains dispersed India Ink (0.0025% India Ink in pure PDMS, mass ratio). All weights are measured using an electronic counting scale balance. Subsequently, appropriate amounts of each stock are mixed into pure PDMS to get the desired TDP and India Ink concentrations. To prepare each mixture, a measured quantity of either India Ink or TDP is added to pure PDMS in a 150mL glass jar. The mixture is then blended using a blade mixer for over 30 minutes. A curing reagent mixture, viz. methyl hydrogenated silica, dimethyl vinylated silica, and trimethylated silica, is added to the suspension to fabricate solid phantoms. The mixture is mixed for 30 minutes, followed by additional mixing for another hour. The curing process starts upon adding the curing agent to the PDMS suspension; the viscosity increases during the mixing process. The mixture is placed in a desiccator for over 2 hours to eliminate trapped air bubbles. Then, the mix is gently poured into bacteriological Petri dishes. The sample is leveled and left to cure slowly at room temperature for 12 hours. The curing process prevents the separation and aggregation of additives that may occur. After heating at 27°, the sample is kept in an oven to a 75° and heated for over 6 hours. Using the process, we developed several recipes as mentioned in the table 4.2

Table 4.2: Phantom Receipes

Recipe 1	
Scattering agent ($Ti0_2$)	**Absorbing agent(India Ink)**
0.5 g TDP	960 μL India Ink
10 g PDMS	10 mL PDMS
33 mL mixture: PDMS 30 mL and 3 mL curing agent (10:1)	
Recipe 2	
Scattering agent ($Ti0_2$)	**Absorbing agent(India Ink)**
50mg TDP	2mL India Ink
4 g PDMS	4 mL(4g) PDMS
11 mL mixture: PDMS 10 mL and 1 mL curing agent (10:1)	
Recipe 3	
Scattering agent ($Ti0_2$)	**Absorbing agent(India Ink)**
30mg TDP	4mL India Ink
4 g PDMS	4 mL(4g) PDMS
11 mL mixture: PDMS 10 mL and 1 mL curing agent (10:1)	

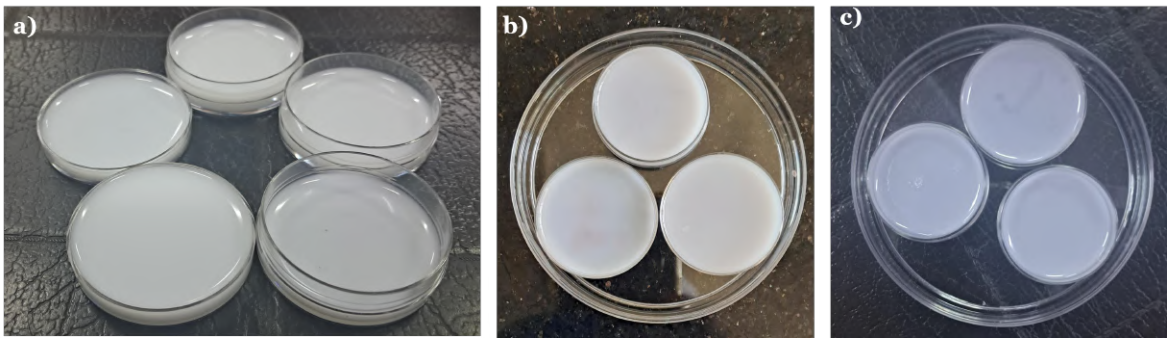

Figure 4.13: Phantoms: a) Recipe 1, b) Recipe 2, and c) Recipe 3.

Chapter 5

Results

The backscattered reflected light from the tissue sample is collected and measured in milli volts (mV) using PDAPC4 photodiode. The measured voltage result for cancerous and adjacent normal tissues is plotted and shown in figure 5.1 for 850 nm, 980 nm, 1270 nm, and 1550 nm wavelengths.

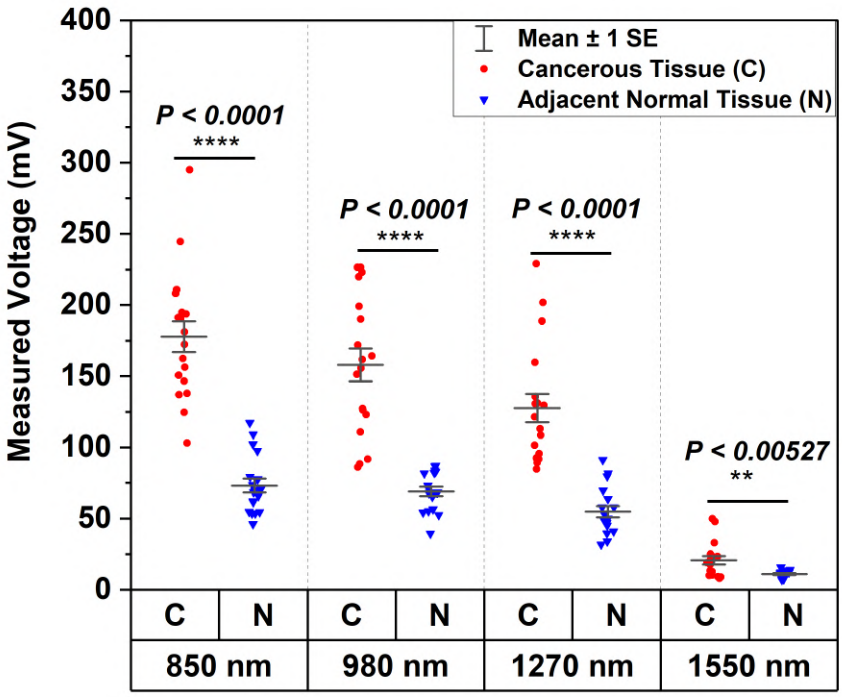

Figure 5.1: Measurements of voltage (mV) for cancerous and adjacent normal tissues using 850nm, 980nm, 1270nm, and 1550nm LASER diodes as illumination sources.

The relative reflectance value for each sample is calculated using equation 4.4, and the measurements are plotted in figure 5.2, 5.3, 5.4, 5.5 for four different wavelengths (850nm, 980nm, 1270nm, and 1550nm).

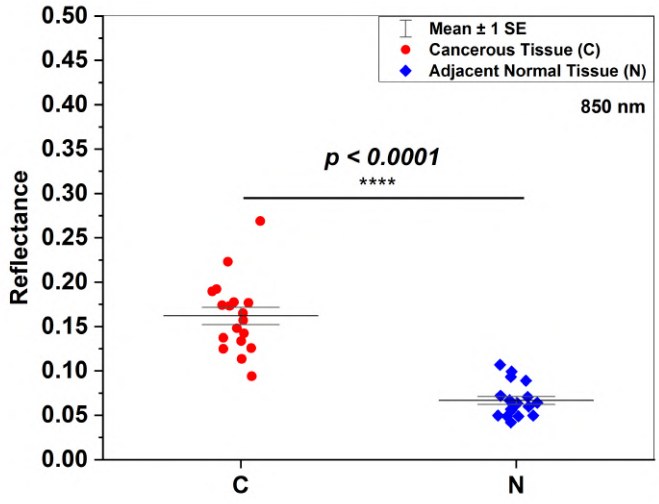

Figure 5.2: Measurement of reflectance in cancerous and adjacent normal tissues using an 850nm LASER diode (L850P010) as the illumination source.

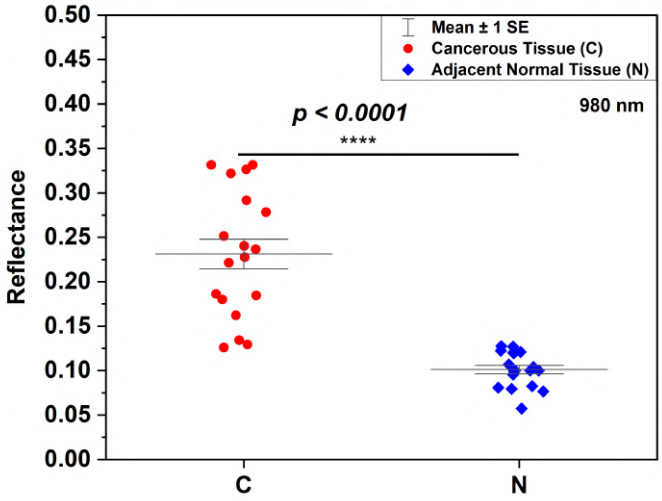

Figure 5.3: Measurement of reflectance in cancerous and adjacent normal tissues using a 980nm LASER diode (L980P010) as the illumination source.

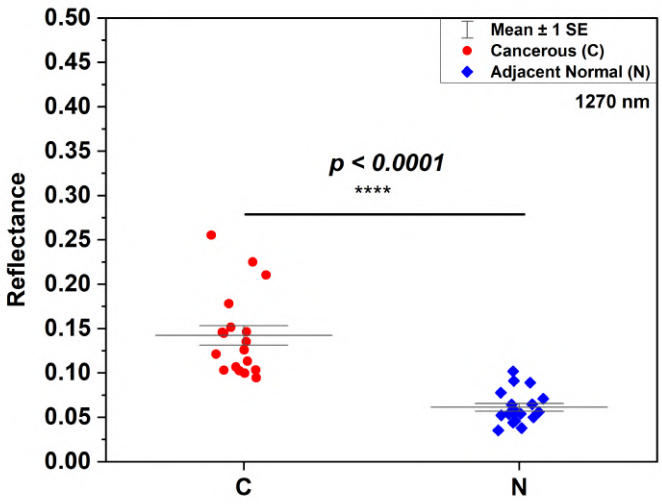

Figure 5.4: Measurement of reflectance in cancerous and adjacent normal tissues using a 1270nm LASER diode (L1270P5DFB) as the illumination source.

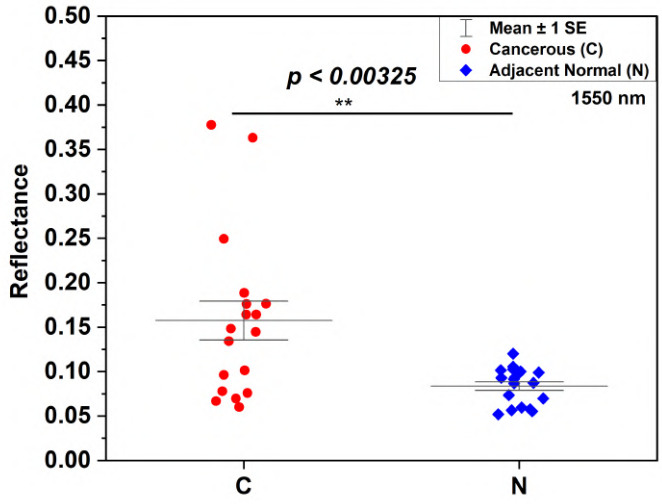

Figure 5.5: Measurement of reflectance in cancerous and adjacent normal tissues using a 1550nm LASER diode (ML925B45F) as the illumination source.

In transmission spectroscopy, absorbance A can be calculated through transmittance T, using equation:

$$A = log(1/T) \tag{5.1}$$

This is based on Beer's law, which states that absorbance is related linearly to the concentration of absorbing structures. Analogously, plot $log(1/R)$ for various wavelengths gives apparent absorption units. The apparent absorption measurement plot for wavelengths of 850nm, 980nm, 1270nm, and 1550nm is shown in figure 5.6.

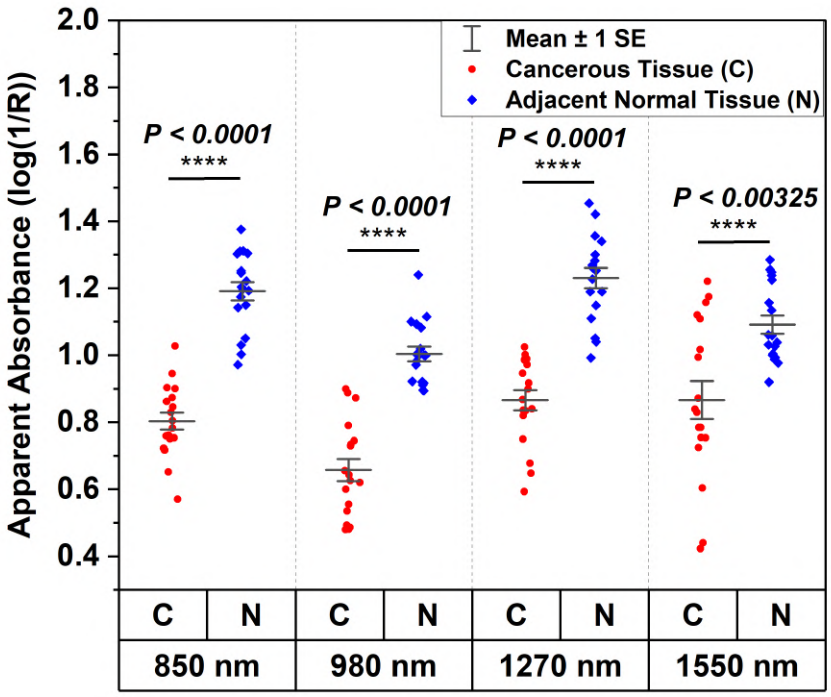

Figure 5.6: Measurements of apparent absorbance (log(1/R)) for cancerous and adjacent normal tissues using 850nm, 980nm, 1270nm, and 1550nm LASER diodes as illumination sources.

Chapter 6

Concluding remarks

6.1 Suggestions for next generation

- **Ergonomics miniaturization:** The probe size can be designed in optimum small size and lighter weight so that the surgeons will ease the surgery and enhance precision.
- **Improved capability in diagnosis:** The more the data, the more the analysis and thus improvement in diagnosis capability. Adding more illumination sources with wavelengths that can provide distinguishable characteristic properties for cancerous and adjacent normal tissue.
- **Machine learning methods:** Incorporating the machine learning algorithms will provide additional robustness to the overall system. Also, incorporating a large amount of data can improve the probe's sensitivity.
- **Wireless transmission and cloud storage:** The transmission can be made wireless for quick and hassle-free data acquisition. The option of storing patient data in cloud storage will make it accessible to the larger medical community, which can help in the proper diagnosis of the patient and further contribute toward the research in the field.
- **Broad applications:** The ESS-based technology can be extended for other cancer diagnoses. Optical properties showing significant changes between cancerous and adjacent normal tissue can be used to delineate cancerous tissue.
- **Power supply:** The system could be improved to operate battery-powered. This allows the system to work in the areas where the supply voltage is unstable.

6.2 Future scope

The intraoperative probe system developed based on Elastic Scattering Spectroscopy(ESS) for breast cancer diagnosis has shown great potential for further advancements and enhancements. The ergonomics of the system, specifically the probe, could be miniaturized to make it hassle-free and easy to use during surgery. Technological advancements in photonics provide the ability to add additional wavelengths, which enhance the accuracy of differentiating various tissues. Furthermore, training machine-learning models can refine diagnostic capability, making decision-making easier and thus reducing the dependence on manual interpretation. The probe system developed can be expanded to other cancer diagnostics, broadening its utility and marking its novelty in oncology. The data transmission could be wireless for seamless system integration between hardware and software. The cloud-storage solutions ease data sharing and enhance collaborative care and outcomes. The experiments are performed on *ex-vivo* tissues; further, the experiments can be carried out on *in-vivo* tissues and intraoperatively.

The probe is handled with a free hand, it can also be operated with a robotic arm for precise shift movement, and it will also ensures the same amount of pressure applied is uniform throughout the experiment. The experiments are carried out on N=18 patients. After a thorough analysis of the optical parameters obtained through data processing, the threshold is set for a quantifying parameter to delineate the tissues. The experiments can be carried out on a large number of samples. More the data, more insightful information can be processed. Power analysis can be carried out to know the number of samples on which the experiments are carried out.

Appendix A

Data

A.1 System parameters

Table A.1: System parameters

Components	**Specifications**
Power supply	230V, 50Hz
System's dimensions	Cubical shape: 251 mm x 251 mm x 81 mm
Operation type	Continuous wave in intervals
Source type	LASER diode
Optical detector	PDAPC4
Portability	Yes
Tissue Type	Formalin-fixed *ex-vivo*

A.2 Cost analysis

The entire cost of the system includes LASER diodes, photo-detector, PCB fabrication, 3D design, and printing.

Table A.2: Cost Analysis

S.no.	**Components**	**Qty**	**Description**	**Vendor**	**Price (INR)**	**Link**
1	BF44LS01-1 to 4 Fan out Bundle	1	1-to-4 Fan-Out Bundle, 400 μ m Core, Low OH, SMA, Round Common End, 1 m Long	THORLABS	38758.22	Link
2	EC4PS - Power Supply Module	1	100 W, +5 V / $\pm$ 12 V Power Supply Module for Custom Electronics Assemblies	THORLABS	20414.73	Link
3	PDAPC4 - Switchable Gain Photodetector	1	InGaAs Switchable Gain Detector on PCB, 800 - 1700 nm, 11 MHz, 3.14 mm^2	THORLABS	25596.55	Link
4	L850P010 - 850 nm LASER Diode	1	850 nm, 10 mW, ϕ5.6 mm, A Pin Code, LASER Diode	THORLABS	2269.68	Link
5	L980P010 - 980 nm LASER Diode	1	980 nm, 10 mW, ϕ5.6 mm, A Pin Code, LASER Diode	THORLABS	2626.88	Link
6	L1270P5DFB - 1270 nm LASER Diode	1	1270 nm, 5 mW, ϕ5.6 mm, D Pin Code, DFB LASER Diode with Aspheric Lens Cap	THORLABS	7636.71	Link

S.no.	Components	Qty	Description	Vendor	Price (INR)	Link
7	ML925B45F - 1550 nm LASER Diode	1	1550 nm, 5 mW, ϕ5.6 mm, D Pin Code, LASER Diode	THORLABS	4764.72	Link
8	Arduino Mega 2560	1	Mega 2560 ATmega2560-16AU Board for Arduino	Sharvi Electronics	1342.56	Link
9	Visible-NIR fibers – probe	1	QR200-7-VIS-BX Part Number: QR200-7-VIS-BX	Ocean Sight	80000	Link
10	SMA couplers	6	Fiber Adapter Square type FTTH Optical Fibre Connector SMA905/906 Coupler	Ebay	1156.75	Link
11	Cooling fan	1	Sunon 4010 5VDC 0.83W Cooling Fan	Robu	299	Link
12	Power Cord	1	1.2M AC 10A 250V Power Supply Adapter Cord Cable EU Plug	Robu	88	Link
13	LASORB L44-47-122-208-X	5	LASORB ESD Absorber for LASER Diode	Pangolin LASER Systems	3130.25	Link
14	LASORB L44-47-121-392-X	2	LASORB ESD Absorber for LASER Diode	Pangolin LASER Systems	1252.10	Link

Appendix B

Program Listing

B.1 Micontroller Code

```
/*
 0.Documentation Section

    Elastic Scattering Spectroscopy Probe

    Runs on Arduino Mega 2560 microcontroller board based on the ATmega2560.
    Inputs: D52 (SW1); D50 (SW2).
    Outputs: D30 (LD_850nm); D28 (LD_940nm); D26 (LD_1270nm); D24 (LD_1550nm); A5 (Blue Light); A6 (Red light); A7 (Green light).

    Pressing SW1 starts the illumination sequence of 1s for all the LASER Diodes.
    t0= 0ms :                 Press SW1 and initially all the LASER diodes are turned "OFF".
    t1= 1ms   to t2= 250ms:   LASER diode with wavelenghth = 850nm turns "ON" and LASER diodes with wavelengths = 940nm, 1270nm, 1550nm are "OFF".
    t3= 251ms to t4= 500ms:   LASER diode with wavelenghth = 940nm turns "ON" and LASER diodes with wavelengths = 850nm, 1270nm, 1550nm are "OFF".
    t5= 501ms to t6= 750ms:   LASER diode with wavelenghth = 1270nm turns "ON" and LASER diodes with wavelengths = 850nm, 940nm, 1550nm are "OFF".
    t7= 751ms to t8= 1000ms:  LASER diode with wavelenghth = 1550nm turns "ON" and LASER diodes with wavelengths = 850nm, 940nm, 1270nm are "OFF".

    Authors: ESS Probe Team
```

```
18      Date: March 27, 2024
19
20      modified 29 March 2024
21      by Kirteyman Singh Rajput
22  */
23  //
24
25
26
27  /*
28    1. Pre-processor Directives Section
29  */
30  #include <Wire.h>
31  #include <Adafruit_ADS1X15.h>
32  Adafruit_ADS1115 ads; /* 16-bit ADC */
33
34
35
36
37  /*
38    2. Global Declarations Section
39  */
40  #define LD_850  30  // LASER Diode of wavelength = 850nm connected to pin
        D30
41  #define LD_940  28  // LASER Diode of wavelength = 850nm connected to pin
        D28
42  #define LD_1270 26  // LASER Diode of wavelength = 850nm connected to pin
        D26
43  #define LD_1550 24  // LASER Diode of wavelength = 850nm connected to pin
        D24
44
45  #define SW_f 52      // Switch 1 is connected to pin D52
46  #define SW_r 50      // Switch 2 is connected to pin D50
47
48  #define RGB_G A7    // Green LED connected to pin A7
49  #define RGB_R A6    // Red LED connected to pin A6
50  #define RGB_B A5    // Blue LED connected to pin A5
51
52  int gui_save;
53  int gui_calibrate;
54
55  // declaring states
```

```
enum States{
  start_state,  // start state
  reset_state,  // calibartion and reset state
  flash_state   // normal operation state
  };
States state = States::start_state;

/*
 3. Subroutines Section
*/

void(* resetFunc)(void) = 0;  //declare reset function @ address 0

// define the next state for the process
void nextState(char userIn) {
  if (userIn == 'c' || (digitalRead(SW_r) && (digitalRead(SW_f) ||
    digitalRead(!SW_f))))
      state = States::reset_state;
  else if (userIn == 's' ||(digitalRead(!SW_r) && digitalRead(SW_f)))
      state = States::flash_state;
  else
      state = States::start_state;
}


// the setup function runs once when you press reset or power the board
void setup() {
  Serial.begin(9600); // baudrate

  pinMode(LD_850, OUTPUT);  // initialize digital pin D30 as an output.
  pinMode(LD_940, OUTPUT);  // initialize digital pin D28 as an output.
  pinMode(LD_1270, OUTPUT); // initialize digital pin D26 as an output.
  pinMode(LD_1550, OUTPUT); // initialize digital pin D24 as an output.

  pinMode(SW_f, INPUT);  // initialize digital pin D52 as an input.
  pinMode(SW_r, INPUT);  // initialize digital pin D50 as an input.

  pinMode(RGB_G, OUTPUT); // initialize digital pin A7 as an output.
  pinMode(RGB_R, OUTPUT); // initialize digital pin A6 as an output.
  pinMode(RGB_B, OUTPUT); // initialize digital pin A5 as an output.

  // ads.begin();    // Initialize ADS1115 ADC (optional)
```

```
97    //  Serial.println("Getting single-ended readings from AIN0");
98    //  Serial.println("ADC Range: +/- 6.144V (1 bit = 3mV/ADS1015, 0.1875mV/
       ADS1115)");
99
100   // The ADC input range (or gain) can be changed via the following
101   // functions, but be careful never to exceed VDD +0.3V max, or to
102   // exceed the upper and lower limits if you adjust the input range!
103   // Setting these values incorrectly may destroy your ADC!
104   //                                                                ADS1015
          ADS1115
105   //                                                                -------
          -------
106   // ads.setGain(GAIN_TWOTHIRDS);  // 2/3x gain +/- 6.144V  1 bit = 3mV
          0.1875mV (default)
107   // ads.setGain(GAIN_ONE);        // 1x gain   +/- 4.096V  1 bit = 2mV
          0.125mV
108   // ads.setGain(GAIN_TWO);        // 2x gain   +/- 2.048V  1 bit = 1mV
          0.0625mV
109   // ads.setGain(GAIN_FOUR);       // 4x gain   +/- 1.024V  1 bit = 0.5mV
          0.03125mV
110   // ads.setGain(GAIN_EIGHT);      // 8x gain   +/- 0.512V  1 bit = 0.25mV
          0.015625mV
111   // ads.setGain(GAIN_SIXTEEN);    // 16x gain  +/- 0.256V  1 bit = 0.125mV
          0.0078125mV
112
113   if (!ads.begin()) {
114     Serial.println("Failed to initialize ADS.");
115     while (1);
116   }
117 }
118
119 // the loop function runs over and over again forever
120 void loop() {
121   //################# 1ST Reading variable declaration ####################
122     int16_t adc[26], adc0[26], adc1[26], adc2[26], adc3[26];
123     float volt=0;
124     float volts0=0;
125     float volts1=0;
126     float volts2=0;
127     float volts3=0;
128
129     float avg=0;
```

```
130     float avg0=0;
131     float avg1=0;
132     float avg2=0;
133     float avg3=0;
134 
135     float sum=0;
136     float sum0=0;
137     float sum1=0;
138     float sum2=0;
139     float sum3=0;
140 
141     char userIn=0;
142 
143     int16_t adc_r[26], adc0_r[26], adc1_r[26], adc2_r[26], adc3_r[26];
144     float volt_r=0;
145     float volts0_r=0;
146     float volts1_r=0;
147     float volts2_r=0;
148     float volts3_r=0;
149 
150     float avg_r=0;
151     float avg0_r=0;
152     float avg1_r=0;
153     float avg2_r=0;
154     float avg3_r=0;
155 
156     float sum_r=0;
157     float sum0_r=0;
158     float sum1_r=0;
159     float sum2_r=0;
160     float sum3_r=0;
161 
162 //#########################2 Reading variable declaration
    ############################
163 
164 
165   int16_t adc_2[26], adc0_2[26], adc1_2[26], adc2_2[26], adc3_2[26];
166     float volt_2=0;
167     float volts0_2=0;
168     float volts1_2=0;
169     float volts2_2=0;
170     float volts3_2=0;
```

```
171
172     float avg_2=0;
173     float avg0_2=0;
174     float avg1_2=0;
175     float avg2_2=0;
176     float avg3_2=0;
177
178     float sum_2=0;
179     float sum0_2=0;
180     float sum1_2=0;
181     float sum2_2=0;
182     float sum3_2=0;
183
184     int16_t adc_r_2[26], adc0_r_2[26], adc1_r_2[26], adc2_r_2[26], adc3_r_2
      [26];
185     float volt_r_2=0;
186     float volts0_r_2=0;
187     float volts1_r_2=0;
188     float volts2_r_2=0;
189     float volts3_r_2=0;
190
191     float avg_r_2=0;
192     float avg0_r_2=0;
193     float avg1_r_2=0;
194     float avg2_r_2=0;
195     float avg3_r_2=0;
196
197     float sum_r_2=0;
198     float sum0_r_2=0;
199     float sum1_r_2=0;
200     float sum2_r_2=0;
201     float sum3_r_2=0;
202
203
204   //################# 3rd Reading variable declaration ###################
205     int16_t adc_3[26], adc0_3[26], adc1_3[26], adc2_3[26], adc3_3[26];
206     float volt_3=0;
207     float volts0_3=0;
208     float volts1_3=0;
209     float volts2_3=0;
210     float volts3_3=0;
211
```

```
212     float avg_3=0;
213     float avg0_3=0;
214     float avg1_3=0;
215     float avg2_3=0;
216     float avg3_3=0;
217 
218     float sum_3=0;
219     float sum0_3=0;
220     float sum1_3=0;
221     float sum2_3=0;
222     float sum3_3=0;
223 
224     int16_t adc_r_3[26], adc0_r_3[26], adc1_r_3[26], adc2_r_3[26], adc3_r_3
        [26];
225     float volt_r_3=0;
226     float volts0_r_3=0;
227     float volts1_r_3=0;
228     float volts2_r_3=0;
229     float volts3_r_3=0;
230 
231     float avg_r_3=0;
232     float avg0_r_3=0;
233     float avg1_r_3=0;
234     float avg2_r_3=0;
235     float avg3_r_3=0;
236 
237     float sum_r_3=0;
238     float sum0_r_3=0;
239     float sum1_r_3=0;
240     float sum2_r_3=0;
241     float sum3_r_3=0;
242 
243 if (Serial.available()>0){
244     userIn = Serial.read();}
245 
246 
247     digitalWrite(RGB_R, LOW);
248     digitalWrite(RGB_B, LOW);
249     digitalWrite(RGB_G, LOW);
250 
251     nextState(userIn);
252     Serial.flush();
```

```
253
254 switch(state){
255
256   case States::start_state:
257     digitalWrite(RGB_G, HIGH);
258     break;
259
260   case States::flash_state:
261     digitalWrite(RGB_B, HIGH);
262
263
264 //#####################################################
265 //############### 1st Reading ########################
266
267       for (int i = 0; i <= 25; i++){
268         adc0_r[i] = ads.readADC_SingleEnded(0);
269       }
270
271
272     digitalWrite(LD_850, HIGH);// LASER diode with wavelength = 850nm turns
     "ON" and LASER diodes with wavelengths = 940nm, 1270nm, 1550nm are "OFF
    "
273     // ADC measurement
274     for (int i = 0; i <= 25; i++){
275         adc0[i] = ads.readADC_SingleEnded(0);
276       }
277     digitalWrite(LD_850, LOW);
278     delay(500);
279
280     for (int i = 0; i <= 25; i++){
281         adc1_r[i] = ads.readADC_SingleEnded(0);
282       }
283
284
285     digitalWrite(LD_940, HIGH);
286     // ADC measurement
287     for (int i = 0; i <= 25; i++){
288         adc1[i] = ads.readADC_SingleEnded(0);
289       }
290     digitalWrite(LD_940, LOW);
291     delay(500);
292
```

```
293
294      for (int i = 0; i <= 25; i++){
295         adc2_r[i] = ads.readADC_SingleEnded(0);
296       }
297
298
299     digitalWrite(LD_1270, HIGH);
300     // ADC measurement
301     for (int i = 0; i <= 25; i++){
302         adc2[i] = ads.readADC_SingleEnded(0);
303       }
304     digitalWrite(LD_1270, LOW);
305     delay(500);
306
307      for (int i = 0; i <= 25; i++){
308         adc3_r[i] = ads.readADC_SingleEnded(0);
309       }
310
311     digitalWrite(LD_1550, HIGH);
312     // ADC measurement
313     for (int i = 0; i <= 25; i++){
314         adc3[i] = ads.readADC_SingleEnded(0);
315       }
316     digitalWrite(LD_1550, LOW);
317
318     // AVERAGING OUT THE READINGS
319     // later use three dimensional array
320
321 //#################################################################
322       for (int i = 0; i <= 25; i++){
323       sum0_r += ads.computeVolts(adc0_r[i])*1000 ;
324       }
325       avg0_r = sum0_r / 26;
326
327
328      for (int i = 0; i <= 25; i++){
329       sum1_r += ads.computeVolts(adc1_r[i])*1000 ;
330       }
331       avg1_r = sum1_r / 26;
332
333
334      for (int i = 0; i <= 25; i++){
```

```
335       sum2_r += ads.computeVolts(adc2_r[i])*1000 ;
336       }
337       avg2_r = sum2_r / 26;
338
339
340      for (int i = 0; i <= 25; i++){
341       sum3_r += ads.computeVolts(adc3_r[i])*1000 ;
342       }
343       avg3_r = sum3_r / 26;
344
345 // ######################################################
346
347
348
349       for (int i = 0; i <= 25; i++){
350       sum0 += ads.computeVolts(adc0[i])*1000 ;
351       }
352       avg0 = sum0 / 26;
353
354
355      for (int i = 0; i <= 25; i++){
356       sum1 += ads.computeVolts(adc1[i])*1000 ;
357       }
358       avg1 = sum1 / 26;
359
360
361      for (int i = 0; i <= 25; i++){
362       sum2 += ads.computeVolts(adc2[i])*1000 ;
363       }
364       avg2 = sum2 / 26;
365
366
367      for (int i = 0; i <= 25; i++){
368       sum3 += ads.computeVolts(adc3[i])*1000 ;
369       }
370       avg3 = sum3 / 26;
371
372
373
374     delay(1000);
375
376
```

```
377 //#####################################################
378 //############### 2nd Reading ########################
379
380
381
382       for (int i = 0; i <= 25; i++){
383         adc0_r_2[i] = ads.readADC_SingleEnded(0);
384       }
385
386
387     digitalWrite(LD_850, HIGH);// LASER diode with wavelength = 850nm turns
     "ON" and LASER diodes with wavelengths = 940nm, 1270nm, 1550nm are "OFF
    "
388     // ADC measurement
389     for (int i = 0; i <= 25; i++){
390         adc0_2[i] = ads.readADC_SingleEnded(0);
391       }
392     digitalWrite(LD_850, LOW);
393     delay(500);
394
395     for (int i = 0; i <= 25; i++){
396         adc1_r_2[i] = ads.readADC_SingleEnded(0);
397       }
398
399
400     digitalWrite(LD_940, HIGH);
401     // ADC measurement
402     for (int i = 0; i <= 25; i++){
403         adc1_2[i] = ads.readADC_SingleEnded(0);
404       }
405     digitalWrite(LD_940, LOW);
406     delay(500);
407
408
409      for (int i = 0; i <= 25; i++){
410         adc2_r_2[i] = ads.readADC_SingleEnded(0);
411       }
412
413
414     digitalWrite(LD_1270, HIGH);
415     // ADC measurement
416     for (int i = 0; i <= 25; i++){
```

```
417         adc2_2[i] = ads.readADC_SingleEnded(0);
418       }
419     digitalWrite(LD_1270, LOW);
420     delay(500);
421 
422      for (int i = 0; i <= 25; i++){
423         adc3_r_2[i] = ads.readADC_SingleEnded(0);
424       }
425 
426     digitalWrite(LD_1550, HIGH);
427     // ADC measurement
428     for (int i = 0; i <= 25; i++){
429         adc3_2[i] = ads.readADC_SingleEnded(0);
430       }
431     digitalWrite(LD_1550, LOW);
432 
433 
434 //#################################################################
435       for (int i = 0; i <= 25; i++){
436       sum0_r_2 += ads.computeVolts(adc0_r_2[i])*1000 ;
437       }
438       avg0_r_2 = sum0_r_2 / 26;
439 
440 
441      for (int i = 0; i <= 25; i++){
442       sum1_r_2 += ads.computeVolts(adc1_r_2[i])*1000 ;
443       }
444       avg1_r_2 = sum1_r_2 / 26;
445 
446 
447      for (int i = 0; i <= 25; i++){
448       sum2_r_2 += ads.computeVolts(adc2_r_2[i])*1000 ;
449       }
450       avg2_r_2 = sum2_r_2 / 26;
451 
452 
453      for (int i = 0; i <= 25; i++){
454       sum3_r_2 += ads.computeVolts(adc3_r_2[i])*1000 ;
455       }
456       avg3_r_2 = sum3_r_2 / 26;
457 
458 // ###################################################
```

```
459
460
461       for (int i = 0; i <= 25; i++){
462       sum0_2 += ads.computeVolts(adc0_2[i])*1000 ;
463       }
464       avg0_2 = sum0_2 / 26;
465
466
467      for (int i = 0; i <= 25; i++){
468       sum1_2 += ads.computeVolts(adc1_2[i])*1000 ;
469       }
470       avg1_2 = sum1_2 / 26;
471
472
473      for (int i = 0; i <= 25; i++){
474       sum2_2 += ads.computeVolts(adc2_2[i])*1000 ;
475       }
476       avg2_2 = sum2_2 / 26;
477
478
479      for (int i = 0; i <= 25; i++){
480       sum3_2 += ads.computeVolts(adc3_2[i])*1000 ;
481       }
482       avg3_2 = sum3_2 / 26;
483       delay(1000);
484
485
486 //#####################################################
487 //############### 3rd Reading ########################
488
489 for (int i = 0; i <= 25; i++){
490         adc0_r_3[i] = ads.readADC_SingleEnded(0);
491       }
492
493
494     digitalWrite(LD_850, HIGH);// LASER diode with wavelength = 850nm turns
     "ON" and LASER diodes with wavelengths = 940nm, 1270nm, 1550nm are "OFF
    "
495     // ADC measurement
496     for (int i = 0; i <= 25; i++){
497         adc0_3[i] = ads.readADC_SingleEnded(0);
498       }
```

```
499     digitalWrite(LD_850, LOW);
500     delay(500);
501 
502     for (int i = 0; i <= 25; i++){
503         adc1_r_3[i] = ads.readADC_SingleEnded(0);
504       }
505 
506 
507     digitalWrite(LD_940, HIGH);
508     // ADC measurement
509     for (int i = 0; i <= 25; i++){
510         adc1_3[i] = ads.readADC_SingleEnded(0);
511       }
512     digitalWrite(LD_940, LOW);
513     delay(500);
514 
515 
516      for (int i = 0; i <= 25; i++){
517         adc2_r_3[i] = ads.readADC_SingleEnded(0);
518       }
519 
520 
521     digitalWrite(LD_1270, HIGH);
522     // ADC measurement
523     for (int i = 0; i <= 25; i++){
524         adc2_3[i] = ads.readADC_SingleEnded(0);
525       }
526     digitalWrite(LD_1270, LOW);
527     delay(500);
528 
529      for (int i = 0; i <= 25; i++){
530         adc3_r_3[i] = ads.readADC_SingleEnded(0);
531       }
532 
533     digitalWrite(LD_1550, HIGH);
534     // ADC measurement
535     for (int i = 0; i <= 25; i++){
536         adc3_3[i] = ads.readADC_SingleEnded(0);
537       }
538     digitalWrite(LD_1550, LOW);
539 
540     // AVERAGING OUT THE READINGS
```

```
541     // later use three dimensional array
542
543 //#################################################################
544       for (int i = 0; i <= 25; i++){
545       sum0_r_3 += ads.computeVolts(adc0_r_3[i])*1000 ;
546       }
547       avg0_r_3 = sum0_r_3 / 26;
548
549
550      for (int i = 0; i <= 25; i++){
551       sum1_r_3 += ads.computeVolts(adc1_r_3[i])*1000 ;
552       }
553       avg1_r_3 = sum1_r_3 / 26;
554
555
556      for (int i = 0; i <= 25; i++){
557       sum2_r_3 += ads.computeVolts(adc2_r_3[i])*1000 ;
558       }
559       avg2_r_3 = sum2_r_3 / 26;
560
561
562      for (int i = 0; i <= 25; i++){
563       sum3_r_3 += ads.computeVolts(adc3_r_3[i])*1000 ;
564       }
565       avg3_r_3 = sum3_r_3 / 26;
566
567 //   ######################################################
568
569
570
571       for (int i = 0; i <= 25; i++){
572       sum0_3 += ads.computeVolts(adc0_3[i])*1000 ;
573       }
574       avg0_3 = sum0_3 / 26;
575
576
577      for (int i = 0; i <= 25; i++){
578       sum1_3 += ads.computeVolts(adc1_3[i])*1000 ;
579       }
580       avg1_3 = sum1_3 / 26;
581
582
```

```
583      for (int i = 0; i <= 25; i++){
584       sum2_3 += ads.computeVolts(adc2_3[i])*1000 ;
585       }
586       avg2_3 = sum2_3 / 26;
587 
588 
589      for (int i = 0; i <= 25; i++){
590       sum3_3 += ads.computeVolts(adc3_3[i])*1000 ;
591       }
592       avg3_3 = sum3_3 / 26;
593 
594 //#########################################################################
595 //############### Averaging all three readings ######################
596 
597     Serial.println(((avg0-avg0_r)+(avg0_2-avg0_r_2)+(avg0_3-avg0_r_3))/3);
598 
599     Serial.println(((avg1-avg1_r)+(avg1_2-avg1_r_2)+(avg1_3-avg1_r_3))/3);
600 
601     Serial.println(((avg2-avg2_r)+(avg2_2-avg2_r_2)+(avg2_3-avg2_r_3))/3);
602 
603     Serial.println(((avg3-avg3_r)+(avg3_2-avg3_r_2)+(avg3_3-avg3_r_3))/3);
604 
605 
606     digitalWrite(RGB_B, LOW);
607     break;
608 
609 
610   case States::reset_state:
611      digitalWrite(RGB_R, HIGH);
612      delay(500);
613      // ADC measurement
614     for (int i = 0; i <= 25; i++){
615         adc[i] = ads.readADC_SingleEnded(0);
616       }
617         for (int i = 0; i <= 25; i++){
618       sum += ads.computeVolts(adc[i])*1000 ;
619       }
620       avg = sum / 26;
621       Serial.print("NO LD ON:");
622       Serial.println(avg);
623 
624      Serial.println("RESET done");
```

```
625       delay(500);
626       resetFunc();  //call reset
627       delay(500);
628       Serial.println("RESET not done");
629       digitalWrite(RGB_R, LOW);
630       break;
631     }
632 }
```

B.2 Flask app

The GUI development in *flask* library of Python consists several .py files. In the process of developing an application for the ESS Probe system, it has *app.py* file, *index.html* file, *mcode.py* file. The mentioned files are scripted below.

B.2.1 app.py

The *app.py* file contains all the function callings and serves the top heirarchy for the GUI application.

```
1  from flask import Flask, render_template
2  from flask.json import jsonify
3  from flask import Flask, render_template, jsonify, request
4  from flask import request
5  import pandas as pd
6  from PIL import Image, ImageTk
7  import tkinter as tk
8  from tkinter import ttk
9  import csv
10 import os
11 import serial
12 import subprocess
13 import mcode as mcode
14 import performance as performance
15 import matplotlib.pyplot as plt
16 import seaborn as sns
17 from io import BytesIO
18 import base64
19
```

```
app = Flask(__name__)

# Sample data for the table
data = []

# Initialize an empty DataFrame to store the table data
table_data = pd.DataFrame(columns=["Column 1", "Column 2", "Column 3"])

def open_and_resize_image(image_path, width, height):
    # Create a dummy root window for image processing
    dummy_root = tk.Tk()
    img = Image.open(image_path)
    img = img.resize((width, height), Image.Resampling.LANCZOS)
    tk_img = ImageTk.PhotoImage(img)
    dummy_root.destroy()  # Close the dummy root window
    return tk_img

@app.route('/')
def home():
    return render_template('index.html')

@app.route('/aim')
def aim():
    return render_template('aim.html')

@app.route('/about')
def about():
    return render_template('about.html')

@app.route('/contact')
def contact():
    return render_template('contact.html')

@app.route('/mcode')
def run_mcode():
    mcode.mcode()
    return render_template('index.html')


@app.route('/mcode1')
def run_mcode1():
    try:
```

```
        result= performance.perform()
        #result = 'Metrics script executed successfully'
        return jsonify(result='success')
    except subprocess.CalledProcessError as e:
        return jsonify(result='error', message=f'Error: {e}')

# Initialize the serial connection with the Arduino
# commPort = 'COM14'
# ser = serial.Serial(commPort, 9600, timeout=1)

# Function to handle the "start" button click event
@app.route('/start', methods=['POST','GET'])
def start():
    if request.method == 'GET':
        import sys, serial, os
        import time
        comm='COM9',
        baudrate = 9600,
        timeout = 0
        ser = serial.Serial('COM9',baudrate=9600,timeout=1)
        time.sleep(2)
        ser.write(b's')
        while True:
            #ser.write(b'g')
            time.sleep(2)

            if ser.in_waiting > 0:
                out = ser.readlines()
                out = [str(i)[2:-5] for i in out]
                data.append(out)
                break

        return jsonify(data=data,result = "success")

        # Send a signal to the Arduino to start sending data
        #ser.write(b'START\n')

        # Read the data from the Arduino and update the table
        #data = ser.readline().decode().strip().split(',')
        #return {'data': data}  # Return the data as JSON to be processed
    by JavaScript

```

```
103
104 # Add a new route to handle saving data to Excel
105 @app.route('/save_data', methods=['POST'])
106 def save_data():
107     try:
108         # Get the JSON data from the request]
109         data_save = request.get_json()
110
111         # Create a DataFrame from the received data
112         headings = data_save[0]  # First element as headings
113         data = data_save[1:]     # Rest of the elements as data rows
114
115 # Create DataFrame with specified headings
116         df = pd.DataFrame(data, columns=headings)
117         df.to_excel('output_final.xlsx', index=False)
118
119         return jsonify({'success': True, 'message': 'Data saved
    successfully'})
120     except Exception as e:
121         return jsonify({'success': False, 'message': str(e)})
122
123 @app.route('/delete_row')
124 def delete_row():
125     # Delete the last item (simulate deleting a row)
126     if data:
127         deleted_row = data.pop()
128         return jsonify(result="success", data=deleted_row)
129     else:
130         return jsonify(result="error", message="No rows to delete")
131
132 @app.route('/send_signal')
133 def send_signal():
134     # Assuming 'ser' is defined globally or in a shared module
135     try:
136         commPort = 'COM9'
137         ser = serial.Serial(commPort, baudrate=9600, timeout=1)
138         ser.write(b'c')
139         # Read the output from Arduino
140         output = ser.readline().decode().strip()
141         ser.close()
142         return "Signal sent successfully!"
143     except Exception as e:
```

```
144         return f"Error sending signal: {str(e)}"
145
146 @app.route('/performance', methods=['POST'])
147 def analysis():
148     try:
149         # Run your performance script using subprocess
150         subprocess.run(['python', 'performance.py'], check=True)
151         result = performance.calculate_performance_metrics()
152
153         return jsonify({'result': 'success', 'message': result})
154     except subprocess.CalledProcessError as e:
155         return jsonify({'result': 'error', 'message': f'Error: {e}'})
156
157 @app.route('/calibrate', methods=['POST'])
158 def calibrate():
159     try:
160         # Run your Python code using subprocess
161         subprocess.run(['python', 'path/to/your/calibration_script.py'],
    check=True)
162         result = 'Calibration script executed successfully'
163
164     except subprocess.CalledProcessError as e:
165         result = f'Error: {e}'
166
167     return {'result': result}
168
169 @app.route('/')
170 def index():
171     left_image_path = "flask_app\static\AllBees.jpg"
172     right_image_path = "flask_app\static\AllBees.jpg"
173     copyright_image_path = "flask_app\static\AllBees.jpg"
174
175     left_image = open_and_resize_image(left_image_path, 100, 100)
176     right_image = open_and_resize_image(right_image_path, 100, 100)
177     copyright_image = open_and_resize_image(copyright_image_path, 50, 50)
178
179     return render_template('index.html', left_image=left_image, right_image
    =right_image, copyright_image=copyright_image)
180
181 if __name__ == '__main__':
182     app.run(host='0.0.0.0', port=5000, debug=True, use_reloader = True)
```

B.2.2 index.html

The *index.html* file contains the skeleton of the application. It has all the routings, aesthetics, physical appearence codes etc.

```
<!DOCTYPE html>
<html lang="en">
<head>
    <meta charset="UTF-8">
    <meta http-equiv="X-UA-Compatible" content="IE=edge">
    <meta name="viewport" content="width=device-width, initial-scale=1.0">
    <link rel="stylesheet" href="{{ url_for('static', filename='style.css')
    }}">
    <title>GUI Development for data Acquisition</title>
    <script src="https://code.jquery.com/jquery-3.6.4.min.js"></script>
    <link rel="stylesheet" href="https://cdnjs.cloudflare.com/ajax/libs/
   font-awesome/4.7.0/css/font-awesome.min.css">
    <style>
      .button-container {
            display: flex;
            flex-direction: column;
            align-items: flex-start;
            justify-content: flex-start;
        }
        .button-container button {
            margin: 5px;
            width: 150px; /* Set a specific width for all buttons */
        }
        .main-container {
            display: flex;
            margin-bottom: 40px;  /* Adjust the margin as needed */
        }
        .footer {
            display: flex;
            align-items: center;
            justify-content: center;
            margin-top: 10px;  /* Adjust the margin as needed */
        }
    </style>
</head>
<body>
    <div>
    <div class="container">
```

```
37          <div class="sidebar">
38              <img src="{{ url_for('static', filename='AllBees.jpg') }}" alt=
    "Bees Lab" class="left-image">
39          </div>
40          <div class="content-final">
41              <h1>Fiber Optic-based Reflectance Probe</h1>
42              <b><p><span style="font-size: medium;">Biomedical and
    Electronics(10^-6 to 10^-9) Engineering Systems Laboratory</span><br/>
43              <span style="font-size: smaller;">solution for big problems lie
     in small things</span></p></b>
44          </div>
45          <div class="sidebar">
46              <img src="{{ url_for('static', filename='NanoFab.png') }}" alt=
    "Nano Fab" class="right-image">
47          </div>
48
49      </div>
50
51      <ul>
52          <li><a class="active2" href="#home" onclick="openCity(event, 'Home
    ')"><i class="fa fa-home"></i>Home</a></li>
53          <li><a href="#aim" onclick="openCity(event, 'Aim')">Aim</a></li>
54          <li><a href="https://labs.dese.iisc.ac.in/beeslab/" target="_blank"
     >Lab Website</a></li>
55          <li><a href="#about" onclick="openCity(event, 'About Us')">About Us
    </a></li>
56          <li style="float:right"><a class="active" href="#contact"
57               onclick="openCity(event, 'Contact Us')"><i class="fa fa-fw fa-
    envelope"></i>Contact Us</a></li>
58      </ul>
59
60      <div id="Aim" class="tabcontent">
61          <p>Breast cancer is the leading cause of cancer in women worldwide,
     with an estimated 2.3 million cases diagnosed in 2020.
62              Elastic Scattering Spectroscopy (ESS) is one of the techniques
    that can potentially diagnose breast tissue during surgery.
63              The handheld breast cancer diagnosis and margin assessment
    system market is in the early stages of its life cycle. The
64              proposed intraoperative probe utilizes the ESS technique to
    provide real-time breast cancer diagnosis and margins
65              assessment intraoperatively</p>
66        </div>
```

```
67
68      <div id="About Us" class="tabcontent">
69        <p>We are M.Tech students, pursuing Electronic Product Design
    curriculum. </p>
70        <p>We work in BEES LAB with Prof. Hardik J. Pandya.</p>
71      </div>
72
73      <div id="Contact Us" class="tabcontent">
74        <p>BEES LAB, Dept. of ESE, IISc, Bangalore.</p>
75        <div id="contactInfo" class="contact-info"></div>
76      </div>
77
78
79     <div class="main-container">
80         <div class="button-container">
81             <button class="start-button" onclick="start()">Start</button>
82             <button class="illuminate-button" onclick="sendSignal()">
    Calibrate</button>
83             <button class="save-button" onclick="saveData()">Save</button>
84             <button class="calibrate-button" onclick="calibrate()">View
    Results</button>
85             <button class="metrics-button" onclick="analysis()">Metrics</
    button>
86             <button class="delete-button" onclick="deleteRow()">Delete</
    button>
87
88         </div>
89
90         <div class="datatable">
91             <table id = "data_table" class="datain">
92                 <thead>
93                     <tr>
94                         <th>850 nm      </th>
95                         <th>980 nm      </th>
96                         <th>1270 nm      </th>
97                         <th>1550 nm      </th>
98                     </tr>
99                 </thead>
100                <tbody>
101                    <!-- Your data rows here -->
102
103                </tbody>
```

```
104             </table>
105         </div>
106 
107         <!-- <div id="metricsResults"></div> -->
108 
109         <div>
110             <h4>Graphs will be displayed here</h4>
111             <div class="image-grid">
112                 <div class="image-item">
113                     <img class="zoom-out" src="{{ url_for('static',
    filename='plots/ScatterPlot.jpg') }}" alt="">
114                 </div>
115                 <div class="image-item">
116                     <img class="zoom-out" src="{{ url_for('static',
    filename='plots/PairPlot.png') }}" alt="">
117                 </div>
118                 <div class="image-item">
119                     <img class="zoom-out" src="{{ url_for('static',
    filename='plots/Heatmap.jpg') }}" alt="">
120                 </div>
121                 <div class="image-item">
122                     <img class="zoom-out" src="{{ url_for('static',
    filename='plots/TruePredicted.jpg') }}" alt="">
123                 </div>
124 
125             </div>
126 
127         </div>
128 
129     </div>
130 </div>
131 
132     <div class="footer">
133         <p>@copyright 2023 |</p>
134         <img src="{{ url_for('static', filename='AllBees.jpg') }}" alt="
    Copyright Image">
135         <p>| Developer: Kumar Raju</p>
136     </div>
137 
138 
139 
```

```
<!-- Add these script tags at the end of your body tag in index.html -->
<script>

    // JavaScript code to handle button click event
    document.getElementById('start-button').addEventListener('click', function() {
        fetch('/start', { method: 'POST' })
            .then(response => response.json())
            .then(data => {
                // Update table with received data
                updateTable(data);
            })
            .catch(error => console.error('Error:', error));
    });

    // Function to update the table with received data
    function updateTable(data) {
        $('tbody').empty();
                // Construct table rows from the updated data and append them to the table body
        data.forEach(function(row) {
            var newRow = '<tr>';
            row.forEach(function(value) {
                newRow += '<td>' + value + '</td>';
            });
            newRow += '</tr>';
            $('tbody').append(newRow);
        });
    }

    function addRow() {
        fetch('/add_row').then(response => response.json()).then(data => {
            if (data.result === "success") {
                let newRow = data.data;
                let tableBody = document.querySelector('tbody');
                let newRowElement = document.createElement('tr');
                newRowElement.innerHTML = `
                    <td>${newRow['Column 1']}</td>
                    <td>${newRow['Column 2']}</td>
                    <td>${newRow['Column 3']}</td>
```

```
                        <td>${newRow['Column 4']}</td>`;
                    tableBody.appendChild(newRowElement);
                }
            });
        }

        function deleteRow() {
            fetch('/delete_row').then(response => response.json()).then(
    data => {
                if (data.result === "success") {
                    let tableBody = document.querySelector('tbody');
                    tableBody.removeChild(tableBody.lastElementChild);
                } else {
                    console.log("No rows to delete");
                }
            });
        }

        function calibrate() {
            fetch('/mcode').then(response => response.json()).then(data =>
    {
                if (data.result === "success") {
                    console.log('success')
                } else {
                    console.log("calibrate failed");
                }
            });
        }

        function analysis() {
            fetch('/mcode1').then(response => response.json()).then(data =>
     {
                if (data.result === "success") {
                    // Access output data and update the display
                    const metricsResults = document.getElementById('
    metricsResults');
                    metricsResults.innerHTML = `<p>${data.output}</p>`;
                    console.log('success');
                } else {
                    console.log('metrics failed');
                }
            })
```

```
216             .catch(error => {
217                 console.error('Error fetching metrics:', error);
218             });
219         }
220 
221         function start() {
222             fetch('/start').then(response => response.json()).then(response
    => {
223                 if (response.result === "success") {
224                     // Access output data and update the display
225                     console.log('success');
226                     updateTable(response.data)
227                 } else {
228                     console.log('start failed');
229                 }
230             })
231             .catch(error => {
232                 console.error('Error :', error);
233             });
234         }
235 
236 
237         function saveData() {
238         // Assuming "tree" is the ID of your Treeview widget
239         var table = document.getElementById('data_table');
240 
241         var data = [Array.from(table.getElementsByTagName('th')).map(header
    => header.textContent.trim())];
242 
243             // Loop through each row in the table body
244             Array.from(table.getElementsByTagName('tbody')[0].
    getElementsByTagName('tr')).forEach(row => {
245                 var rowData = [];
246                 // Loop through each cell in the row and extract the text
    content
247                 Array.from(row.getElementsByTagName('td')).forEach(cell =>
    {
248                     rowData.push(cell.textContent);
249                 });
250                 data.push(rowData);
251             });
252         console.log(data)
```

```
253         // Send an AJAX request to the Flask route
254         $.ajax({
255             type: 'POST',
256             url: '/save_data',
257             contentType: 'application/json;charset=UTF-8',
258             data: JSON.stringify(data),
259             success: function (response) {
260                 if (response.success) {
261                     alert(response.message);
262                 } else {
263                     alert('Error saving data: ' + response.message);
264                 }
265             },
266             error: function () {
267                 alert('Error saving data.');
268             }
269         });
270     }
271 
272         function sendSignal() {
273             // You can use JavaScript to make an AJAX request to trigger
    the route
274             fetch('/send_signal')
275                 .then(response => response.text())
276                 .then(message => alert(message))
277                 .catch(error => console.error('Error:', error));
278         }
279 
280         document.getElementById('calibrateButton').addEventListener('click'
    , function() {
281             fetch('/calibrate', {
282                 method: 'POST',
283             })
284             .then(response => response.json())
285             .then(data => {
286                 console.log(data.result);
287                 // Handle the result as needed
288             })
289             .catch(error => {
290                 console.error('Error:', error);
291             });
292         });
```

```
        function openCity(evt, iconname) {
            // Declare all variables
            var i, tabcontent;
        // Get all elements with class="tabcontent" and hide them
            tabcontent = document.getElementsByClassName("tabcontent");
            for (i = 0; i < tabcontent.length; i++) {
                tabcontent[i].style.display = "none";
            }

        // Show the current tab, and add an "active" class to the button
    that opened the tab
        document.getElementById(iconname).style.display = "block";
        evt.currentTarget.className += " active";
        }

        function navigatetothis() {
            // Change the URL to the external website
            window.location.href = 'https://labs.dese.iisc.ac.in/beeslab/';
        }

    </script>
   <!-- <script src="{{ url_for('static', filename='script.js') }}"></
    script> -->
</body>
</html>
```

B.2.3 mcode.py

```
# -*- coding: utf-8 -*-
#This is the code for mUA and mUS values starting from 1 to 5 and 1 to 50
"""Kumar.ipynb

Automatically generated by Colaboratory.

Original file is located at
    https://colab.research.google.com/drive/1kBMn8tcS0Tx_NaK-
    Ndpvag9AhhFGTHQo
"""

import math
import numpy as np
```

```
import pandas as pd
import seaborn as sns
import matplotlib.pyplot as plt

def gama(mua,mus):
  return 2 * (mua/mus)

def Reflectens(mua,mus):
  ga = gama(mua,mus)
  p1=1.25
  g=0.9
  ro=0.4
  pi = math.pi
  return round(((0.75)**g /pi) * 10**(-1-p1*ga) * ((mus**2*(1-g)**g)/((mus*
    ro)**(1+ga))) * math.exp(-ga),6)

def mcode():
  mua_start=1
  mua_end=5
  mua_step=0.01
  muas = np.arange(mua_start, mua_end, mua_step)
  l=len(muas)
  #print(l)
  #print("Absorption coefficient : ",muas)
  print()

  mus_start=5
  mus_end=60
  mus_step=0.05
  muses = np.arange(mus_start,mus_end,mus_step)
  m=len(muses)
  #print(m)
  #print("Scattering Coefficient : " , muses)
  print()


  result = []
  a=open("Exp1.txt","w")
  original_values=[]
  for mus in muses:
    for mua in muas:
      vals = Reflectens(mua,mus)
```

```
54      result.append(vals)
55      original_values.append(vals)
56    a.write(f"For mus : {mus} = "+str(result)+"\n")
57    result=[]
58  a.close()
59  #print("Original Values : ",original_values)
60  original_values = [round(val*100, 5) for val in original_values]  #
     Assuming 5 significant figures
61  print()
62
63  #importing pandas as pd
64
65  # Read and store content
66  # of an excel file
67  read_file = pd.read_excel ("output_final.xlsx")
68
69  # Write the dataframe object
70  # into csv file
71  read_file.to_csv ("Exp1.csv",
72          index = None,
73          header=None)
74
75  data = open("Exp1.csv","r")
76  datapoints = data.readlines()
77  print(datapoints)
78
79  # Define normalization factors for each wavelength
80  normalization_factors = {
81      850: 90879.82,    # Normalization factor for 850nm
82      980: 85795.67,    # Normalization factor for 980nm
83      1270: 85795.67,   # Normalization factor for 1270nm
84      1550: 18021.63   # Normalization factor for 1550nm
85  }
86
87  # Normalize the data using the corresponding normalization factor for
     each wavelength
88  total_data = []
89  for line in datapoints:
90      data_values = [float(value) / normalization_factors[wavelength]
91                     for value, wavelength in zip(line.split(','), [850,
     980, 1270, 1550]) if value.strip() != '']
92      total_data.append(data_values)
```

```
print(total_data)

experimental_values = []
for i in total_data:
  experimental_values+=i
data.close()


# print("Experimental Values : ",experimental_values)
print()

final = open("result_exp1.csv","w")


# Open the final_result.csv file for writing
with open("result_exp1.csv", "w") as final:
    # Write column headers
    final.write("Original Reflectance,Experimental Reflectance,Minimum MSE,Mua Value,Mus Value\n")

    for i in range(len(experimental_values)):
        x = np.array(original_values)
        y = np.array([experimental_values[i]] * (l*m))
        mse = ((x - y)**2)

        # Find the index of the minimum MSE value
        index = np.argmin(mse)
        mua_index = index // m
        mus_index = index % m

        # Write data to the file
        final.write(f"{original_values[i]},{experimental_values[i]},{min(mse)*(10**7)},{muas[mua_index - 1]},{muses[mus_index - 1]}\n")



# Load the data from the final_result.csv file
data = pd.read_csv("result_exp1.csv")

# Add a new column 'Tissue Type' based on the threshold
threshold_exp = 0.5  # threshold value for experimental reflectance
threshold_mus = 25 # threshold value for scattering coefficient
```

```
133 data['Tissue Type'] = np.where((data['Experimental Reflectance'] <
     threshold_exp) | (data['Mus Value'] < threshold_mus), 'Normal', '
     Cancerous',)
134
135 # Scatter Plot
136 plt.figure(figsize=(10, 6))
137 sns.scatterplot(x="Mus Value", y="Mua Value", data=data, hue="Tissue Type
     ", style="Tissue Type", sizes=(20, 200))
138 #plt.plot([0, max(data["Mus Value"])], [0, max(data["Mua Value"])],
     linestyle="--", color="red", label="45-degree line")
139 plt.title("Scatter Plot of Experimental Reflectance")
140 plt.xlabel("Mus Value")
141 plt.ylabel("Mua value")
142 plt.legend(title="Tissue Type")
143 plt.savefig('static\plots\ScatterPlot.jpg')
144 #plt.show()
145
146 # Pair Plot
147 pair_plot = sns.pairplot(data, hue="Tissue Type", vars=["Experimental
     Reflectance", "Minimum MSE", "Mua Value", "Mus Value"], palette="viridis
     ", height=2)
148 plt.suptitle("Pair Plot of Experimental, Minimum MSE, Mua, and Mus Values
     ", y=1)
149 # Define custom labels for x and y axes
150 x_labels = ["Exp. Reflectance", "Minimum MSE", "Mua Value", "Mus Value"]
151 y_labels = ["Exp. Reflectance", "Minimum MSE", "Mua Value", "Mus Value"]
152
153 # Iterate over each subplot and set custom labels
154 for i in range(len(pair_plot.axes)):
155     for j in range(len(pair_plot.axes)):
156         pair_plot.axes[i, j].set_xlabel(x_labels[j])
157         pair_plot.axes[i, j].set_ylabel(y_labels[i])
158 plt.savefig('static\plots\PairPlot.png')
159 #plt.show()
160
161 # Handle duplicate entries by aggregating the values (you may use a
     different aggregation method)
162 data_grouped = data.groupby(['Mua Value', 'Mus Value', 'Tissue Type']).
     agg({'Experimental Reflectance': 'mean'}).reset_index()
163
164 # Drop duplicate index-column combinations
165 data_grouped = data_grouped.drop_duplicates(subset=['Mua Value', 'Mus
```

```
    Value'])
166
167 # Heatmap
168 heatmap_data = data_grouped.pivot(index="Mus Value", columns="Mua Value",
      values="Experimental Reflectance")
169 # Check if there are any NaN values
170 if heatmap_data.isna().sum().sum() > 0:
171     # If there are NaN values, fill them with some default value or use
    interpolation
172     heatmap_data = heatmap_data.fillna(0)  # You might want to replace 0
    with another suitable value
173
174 plt.figure(figsize=(12, 8))
175 sns.heatmap(heatmap_data, cmap="viridis", annot=True, fmt=".2f", cbar_kws
    ={'label': 'Experimental Reflectance'})
176 plt.title("Heatmap of Experimental Reflectance")
177 plt.xlabel("Mua Value")
178 plt.ylabel("Mus Value")
179 # Round the numeric labels to two decimal places
180 plt.xticks(ticks=range(len(heatmap_data.columns)), labels=[round(label,
    2) for label in heatmap_data.columns])
181 plt.yticks(ticks=range(len(heatmap_data.index)), labels=[round(label, 2)
    for label in heatmap_data.index])
182 plt.savefig('static\plots\HeatMap.jpg')
183 #plt.show()
184
185 # Scatter plot between Predicted Reflectance and True Reflectance
186 plt.figure(figsize=(10, 6))
187 sns.scatterplot(x="Original Reflectance", y="Experimental Reflectance",
    data=data, label="Experimental Reflectance", marker="o")
188 sns.scatterplot(x="Original Reflectance", y="Original Reflectance", data=
    data, label="Original Reflectance", marker="x")
189 plt.plot([0, max(data["Original Reflectance"])], [0, max(data["Original
    Reflectance"])], linestyle="--", color="red", label="45-degree line")
190 plt.xlim([0, 1])
191 plt.ylim([0, 1])
192 plt.title("Scatter Plot of True Reflectance vs Predicted Reflectance")
193 plt.xlabel("True Reflectance")
194 plt.ylabel("Predicted Reflectance")
195 plt.legend()  # Show legend
196 plt.savefig('static\plots\TruePredicted.jpg')
197 #plt.show()
```

Appendix C

Contributions

In the process of completing the project, various contributions have been executed, and some have significant novelty and may have the potential for Intellectual property. The design of the intraoperative system itself, which includes the PCB design and ergonomic design, involves multiple wavelengths of LASER diodes for characterizing the breast biopsy tissues.

The optical configuration and arrangement of specific components like LASER diodes, LASORB ESD protection diodes, PDAPC4 photodetector, the algorithms developed for data processing, analysis of optical parameters viz. reflectance, scattering coefficient, and absorption coefficient. The application of elastic scattering spectroscopy (ESS) for the intraoperative system is a novelty for diagnosing breast cancer.

Bibliography

[1] Ocean Insight. Reflection or backscatter probe qr200-7-vis-bx. *datasheet*.

[2] Thor Labs. Pdapc4 - ingaas switchable gain detector on pcb, 800 - 1700 nm, 11 mhz, 3.14 mm^2. *datasheet*, May 13, 2021.

[3] David W. Allen Kimberly A. Briggman Aaron M. Goldfain, Paul Lemaillet and Jeeseong Hwang. Polydimethylsiloxane tissue-mimicking phantoms with tunable optical properties. *Journal of Biomedical Optics*, 27(7), 2021.

[4] Inc. National Breast Cancer Foundation. Understanding breast cancer, 2024. https://www.nationalbreastcancer.org/what-is-cancer/.

[5] National Breast Cancer Foundation. Breast cancer anatomy and how breast cancer starts, 2024. https://nbcf.org.au/about-breast-cancer/diagnosis/breast-cancer-anatomy/.

[6] National Breast Cancer Foundation. Breast anatomy, 2024. https://www.nationalbreastcancer.org/breast-anatomy/.

[7] Cleveland Clinic. Breast anatomy, 2024. https://my.clevelandclinic.org/health/articles/8330-breast-anatomy.

[8] Inc. National Breast Cancer Foundation. Types of breast cancer, 2023. https://www.nationalbreastcancer.org/types-of-breast-cancer/.

[9] Inc. National Breast Cancer Foundation. Symptoms of breast cancer, 2023. https://www.nationalbreastcancer.org/breast-cancer-symptoms-and-signs/.

[10] Global Cancer Observatory. International agency for research on cancer, 2022. https://gco.iarc.who.int/en.

[11] Thorlabs. *ECM Series ACDC Power adapter*.

[12] E. Boichenko and D. Kirsanov. Optical spectroscopy and chemometrics in intraoperative tumor margin assessment. *TrAC Trends in Analytical Chemistry*, page 116955, 2023.

[13] M. Thill. Intraoperative margin assessment during breast-conserving surgery by using radiofrequency spectroscopy. *CA:A cancer journal for clinicians*, 10(3):301–315, 2013.

[14] L. Lazard. Towards mm-wave spectroscopy for dielectric characterization of breast surgical margins. 45:64–69, 2019.

[15] Vingiani A. Di Pietro S. Martellosio A. Espin-Lopez P.F. Di Meo S. Pasian M. Ghitti M. Mangiacotti M. Sacchi R. Summers, P.E. and P. Veronesi. New Technique Renders Underarm Surgery Unnecessary for 80

[16] Santa Maria P.L. Wijesinghe P. Francis Kennedy B.-Allardyce B.J. Eikelboom R.H. Atlas M.D. Tan, H.E.I. and R.J. Dilley. Optical coherence tomography of the tympanic membrane and middle ear: a review. OtolaryngologyaHead and Neck Surgery. 159(3):424–438, 2018.

[17] Price E.L. Publicover-Brouwer P. Matheson K. Ly-T.Y. Pasternak S. Walsh N.M. Gallant C.J. Oakley A. Hull P.R. MacLellan, A.N. and R.G. Langley. The use of noninvasive imaging techniques in the diagnosis of melanoma: a prospective diagnostic accuracy study. *Journal of the American Academy of Dermatology*, 85(2):353–359, 2021.

[18] Gadd M.A. Lanahan-C.R. Rai U. Tang R.-Rice-Stitt T. Merrill A.L. Strasfeld D.B. Ferrer J.M. Brachtel E.F. Smith, B.L. and M.C. Specht. Real-time, intraoperative detection of residual breast cancer in lumpectomy cavity walls. *Breast cancer research and treatment*, 171:413–420, 2018.

[19] Hofvind S. Skaane, P. and A. Skjennald. Randomized trial of screen-film versus full-field digital mammography with soft-copy reading in population-based screening program: follow-up and final results of Oslo II study. *Radiology*, 244(3):708–717, 2007.

[20] Waters J. Morrow, M. and E. Morris. MRI for breast cancer screening, diagnosis, and treatment. *The Lancet*, 378(9805):1804–1811, 2011.

[21] Thorlabs. *L850P010, 850nm, 5.6mm, TO-18 can package discreet laser diode*, 2010. `https://www.thorlabs.com/thorproduct.cfm?partnumber=L850P010`.

[22] Thorlabs. *L980P010, 980nm, 5.6 mm TO Can Laser Diode*, 2013. https://www.thorlabs.com/thorproduct.cfm?partnumber=L980P010.

[23] Thorlabs. *L1270P5DFB, 1270nm, DFB Laser Diode, 5 mW*, 2023. https://www.thorlabs.com/thorproduct.cfm?partnumber=L1270P5DFB.

[24] Thorlabs. *ML9xx45 SERIES, 1550nm, Laser Diodes*, 2004. https://www.thorlabs.com/thorproduct.cfm?partnumber=ML925B45F.

[25] Thorlabs. *PDAPC4 - InGaAs Switchable Gain Detector on PCB, 800 - 1700 nm, 11 MHz BW*, 2021. https://www.thorlabs.com/thorproduct.cfm?partnumber=PDAPC4.

[26] Oceaninsight. *QR200-7-VIS-BX, Reflection/backscatter probe*, 2024. https://www.oceaninsight.com/products/fibers-and-probes/probes/reflectionbackscatter-probes/qr200-7-vis-bx/.

[27] Tengfei Sun1 and Daqing Piao. Diffuse photon remission associated with the center-illuminated-area-detection geometry: Part I, an approach to the steady-state model. *Applied Optics*, 61(31), 2022.

[28] Thorlabs. *BF44LS01 - 1-to-4 Fan-Out Bundle, 400 µm Core, Low OH, SMA, Round Common End, 1 m Long*. https://www.thorlabs.com/thorproduct.cfm?partnumber=BF44LS01.

[29] Ebay. *2pcs Fiber Adapter Square type FTTH Optical Fibre Connector SMA905/906 Coupler*, 2024. https://www.ebay.com/itm/393618794146?_ul=IN.

[30] Texas Instruments. *Ultra-Small, Low-Power, 16-Bit Analog-to-Digital Converter with Internal Reference*, 2009. https://cdn-shop.adafruit.com/datasheets/ads1115.pdf.